Title
Bayesian inference of rock strength anisotropy: Uncertainty analysis of the Hoek–Brown failure criterion

Authors
Gomes, Guilherme JC
Forero, John H
Vargas, Eurípedes A
et al.

Publication Date
2021-12-01

DOI
10.1016/j.ijrmms.2021.104952

Peer reviewed

International Journal of Rock Mechanics & Mining Sciences 148 (2021) 104952

Contents lists available at ScienceDirect

International Journal of Rock Mechanics and Mining Sciences

journal homepage: www.elsevier.com/locate/ijrmms

Bayesian inference of rock strength anisotropy: Uncertainty analysis of the Hoek–Brown failure criterion

Guilherme J.C. Gomes [a,b,*], John H. Forero [c], Eurípedes A. Vargas Jr. [c], Jasper A. Vrugt [d,e]

[a] Graduate Program in Geotechnics, School of Mines, Federal University of Ouro Preto, Ouro Preto, Minas Gerais, Brazil
[b] Department of Environmental Engineering, Federal University of Ouro Preto, Minas Gerais, Brazil
[c] Department of Civil Engineering, Pontifical Catholic University of Rio de Janeiro, Rio de Janeiro, Brazil
[d] Department of Civil and Environmental Engineering, University of California, Irvine, CA, USA
[e] Department of Earth System Science, University of California, Irvine, CA, USA

ARTICLE INFO

Keywords:
Anisotropic rocks
Hoek–Brown strength criterion
Uncertainty analysis
Bayesian inference
Model calibration

ABSTRACT

Strength properties of most sedimentary and metamorphic rocks are known to vary with direction. Knowledge of this so-called rock anisotropy is of utmost importance for reliability analysis and engineering design. The purpose of this paper is twofold. First, we propose a formulation of the Hoek–Brown (HB) failure criterion, which calculates strength anisotropy using a non-uniform scaling of the stress tensor. We use two scaling factors, C_N and C_S, to link the orientation of the anisotropy planes with the loading direction. As we assume isotropic parameters for intact rock, our HB model formulation is relatively easy to use and has the additional advantage that it does not demand any modifications to the HB failure criterion. Second, we embed our HB model formulation in a Bayesian framework and illustrate its power and usefulness using experimental data of anisotropic rock samples published in the literature. Results demonstrate that our HB model formulation predicts accurately measured peak strengths of rocks with different degrees of anisotropy, confining stresses and anisotropy orientations. The uncertainty in peak strength of anisotropic rocks can be quite large, reiterating the need for an explicit treatment of strength anisotropy uncertainty in rock mechanics studies. The Bayesian methodology is general-purpose, and, as such, can help better inform geotechnical engineers, contractors and other professionals about rock conditions and design reliability and assist decision makers in determining the overall risks of engineering structures.

1. Introduction

Most metamorphic and sedimentary rocks are anisotropic meaning that their physical properties vary with direction when subjected to stress. Rock anisotropy is the result of a myriad of tectonic,[1–3] deposition,[4] stress state and history,[5] and fabric[6] processes. These processes are usually characterized as mineral foliation in metamorphic rocks and stratification in their sedimentary counterparts and produce anisotropic planes in sandstone, shale, slate, marble, schist, gneiss, and phyllite. In large rock masses, planes of anisotropy are also classified as discontinuities and/or fractures. Experimental evidence suggests that the strength properties of anisotropic rocks depend critically on the orientation of stresses or loads with respect to their anisotropic planes.[7–14] As anisotropy exerts a large control on the stability and strength of geotechnical structures, including dam and bridge foundations,[1,15] underground excavations,[16] oil boreholes[17,18] nuclear waste storage,[19] and slopes,[20,21] accurate estimates of rock strength anisotropy are of utmost importance in rock engineering design.[15,22–25] Stability analysis of such structures should take into account the influence of structural anisotropy on the mechanical behavior of rocks.

Engineers often make use of strength criteria to model rock anisotropy. During the last few decades, a great deal of research has been dedicated to the development and formulation of constitutive models for rock anisotropy and failure criteria of geomaterials.[22,26–28] Much of this research has been inspired by the classical theories of Navier–Coulomb and Griffith, and has led to theoretical[8,26,29–31] and/or empirical strength criteria.[11] An example of theoretical strength criteria includes the single plane of weakness criterion of Jaeger,[29] which relies on the classic Mohr–Coulomb criterion to describe rock failure using two different sets of material constants (cohesion and friction angle) along both the plane of weakness and intact rock. This criterion models the strength behavior of a rock cut by one joint or a single joint set relatively well.[32] Jaeger's theory was extended to highly

* Corresponding author at: Graduate Program in Geotechnics, School of Mines, Federal University of Ouro Preto, Ouro Preto, Minas Gerais, Brazil.
E-mail addresses: guilhermejcg@ufop.edu.br (G.J.C. Gomes), jforerogga_11@hotmail.com (J.H. Forero), vargas@puc-rio.br (E.A. Vargas Jr.), jasper@uci.edu (J.A. Vrugt).

https://doi.org/10.1016/j.ijrmms.2021.104952
Received 24 February 2021; Received in revised form 8 July 2021; Accepted 28 October 2021
Available online 17 November 2021

stratified materials by Ref. 33 and for transversely isotropic rocks by Ref. 34. Yet, these last two criteria are defined with several material parameters. Theoretical strength criteria based on Mohr–Coulomb criterion also include continuous variation of friction angle,[26] cohesion[29] and both Mohr–Coulomb parameters[8] with anisotropy direction. Other commonly used theoretical failure criteria based on the Griffith theory include the Walsh–Brace[31] and Hoek[30] fracture anisotropic theories. This body of research has shown that failure criteria can be formally modified to take into account the anisotropy in strength properties, however the applicability of these approaches is restricted as these models are unable to accurately describe rock failure.[34,35] Moreover, some of the coefficients (parameters) of theoretical strength criteria cannot be measured directly from rock specimens and, therefore, are difficult to determine in practical applications,[21] particularly for larger rock masses. Consequently, researchers and practitioners often resort to empirical strength criteria instead.

In the past decades many different publications have appeared in the rock mechanics literature on the development and use of empirical strength criteria[11,36–38]. Most of these criteria are derived from first principles and/or closed-form equations and require experimental data from rock specimens (e.g. triaxial compression testing) to determine the unknown parameters of relevant failure criteria using linear and/or nonlinear regression techniques.[15] What is more, the usefulness of empirical criteria is often limited to the rock types that they have been developed for.[39] Among the different empirical strength criteria, the Hoek–Brown (HB) criterion[11,40] is most widely used for determining the strength of both intact rock and rock masses[35] including applications to engineering structures such as tunnels[41] and slopes.[42,43] The HB criterion is particularly appealing as it considers different rock properties (structure, strength and stress state), can handle nonlinear failure envelopes and can be adapted to provide an estimate of the decreased strength of the rock mass[44,45] using parameters that can be determined from laboratory experiments. For these reasons, the HB strength criterion and constitutive relationships, hereafter conveniently referred to as the HB model, have found its way into commercial geotechnical software packages such as PLAXIS and FLAC.

The HB model was originally developed for isotropic geomaterials; hence, further developments are needed to warrant its application to anisotropic materials/rocks. A simple adaptation to anisotropic rocks involves the use of non-isotropic HB model parameters,[46–48] but additional research is needed to determine their suitability to other anisotropic rock types.[49] Such redefinition of the HB model parameters may be convenient, but is susceptible to misinterpretation in practical application of anisotropic HB strength criteria.[49] Therefore, an anisotropic strength criterion that preserves the isotropic formulation of the HB model could be a valuable contribution to engineering practice. Indeed, Ref. 13 proposed a one-parameter extension of the HB strength criterion to account for strength anisotropy. Unfortunately, as this parameter does not originate from first principles and cannot be measured directly in physical experiments, a large number of experiments are required to accurately determine its value using statistical inference.[50]

Published modifications of the HB model may succeed in accurately predictingthe strength and failure of anisotropic rock specimens, yet current practice fails to systematically address the uncertainty of HB model parameters and output.[51] Regression methods may suffice in finding the optimum, least squares values, of the HB parameters, from measured stress data of anisotropic rock samples. It would be naive, however, to rely on such single unique estimates of the parameters in the presence of structural imperfections of the HB failure criterion and constitutive relationships (epistemic uncertainty), natural variability and measurement errors of the experimental data (aleatory uncertainty).[52] Indeed, practical experience suggests that it is typically difficult to find a single "best" vector of parameter values, whose performance obviates consideration from other feasible solutions. Therefore, we should dissect and delineate properly the space of adequate solutions. This approach is not only key to (among others) analysis of parameter identifiability and quantification of the uncertainty associated with the simulated model output, but also of utmost importance for engineering design and reliability analysis. In fact, some countries are shifting the focus from the use of safety factors to more reasonable reliability-design standards for engineering works.[53,54] Hence, there is sufficient scope and reason to develop more comprehensive, uncertainty-based, approaches for the characterization and analysis of rock strength anisotropy.

There is a growing awareness in the geotechnical community about the importance of uncertainty quantification as researchers are trying to quantify design reliability and inform geotechnical engineers, contractors and other professionals about soil and rock conditions and decision makers seek to better determine the overall technical and financial risks of engineering structures and mitigate geotechnical-related risks.[51,53,55–59] This paper builds on our recent work on slope stability analysis, which embraced uncertainty analysis of safety factors to improve risk analysis and decision-making.[60,61] Recent publications in the rock engineering literature have introduced methods for assessing the uncertainty of *in situ* stress data,[58,62] rock mass properties[63–65] and slope stability,[56,66] including its application to the design of foundations,[67] tunnels[68] and gas reservoirs.[69] Many of these contributions adopted a Bayesian approach to reconciling rock engineering models with field and/or laboratory data. For example, Ref. 51 used Bayesian inference to estimate the intact rock strength from data of compressive and tensile strength tests. This work demonstrated the advantages of the Bayesian approach over standard Frequentist regression methods for uncertainty quantification of model parameters and output. Nevertheless, as Ref. 45 has shown, differences between the inferred strength envelopes of both methods may be small in practical applications. Another recent study by Ref. 70 used Bayesian inference to back out the twelve coefficients of the Lade–Kim isotropic model using a non-uniform scaling of the stress tensor[71] and two scaling factors, C_N and C_S, that link the orientation of the anisotropy planes with the loading direction. The maximum deviatoric stresses and stress–strain curves predicted and simulated by their model were shown to be in good agreement with experimental data, but the authors did not present and investigate the uncertainty of the predicted maximum deviatoric stresses. What is more, the so-called posterior estimates of C_N and C_S were evaluated only for two sedimentary rocks, leaving unanswered the question of how well these inferred scaling factors generalize to other anisotropic rocks?

In this paper, we introduce an alternative formulation of the HB model for anisotropic rocks. Our approach builds on the isotropic HB failure criterion and calculates the strength anisotropy using a non-uniform scaling of the stress tensor. We follow Ref. 70 and use the scaling factors, C_N and C_S, to link the orientation of the planes of anisotropy with the loading direction. Our HB model formulation assumes isotropic parameters for intact rock, which can be measured directly from rock samples using triaxial tests. This approach is relatively easy to use and has the additional advantage that it does not demand any modifications to the HB failure criterion. We illustrate our anisotropic HB formulation by application to experimental data of anisotropic rock samples published in the literature. This includes experiments with different confining stresses and anisotropy orientations. The optimum anisotropic model parameters and their underlying statistical uncertainty (posterior distribution) are inferred from Bayesian analysis using Markov chain Monte Carlo (MCMC) simulation with the DREAM algorithm[72–74]. Specific attention is paid to the posterior distribution of our HB model formulation. The predicted rock strengths are evaluated using split sampling with a calibration and evaluation data set. Furthermore, the posterior model simulations are investigated using standard error (residual) metrics and the 95% confidence intervals of the HB model output are determined to clarify the predictive uncertainty of modeled rock strength anisotropy.

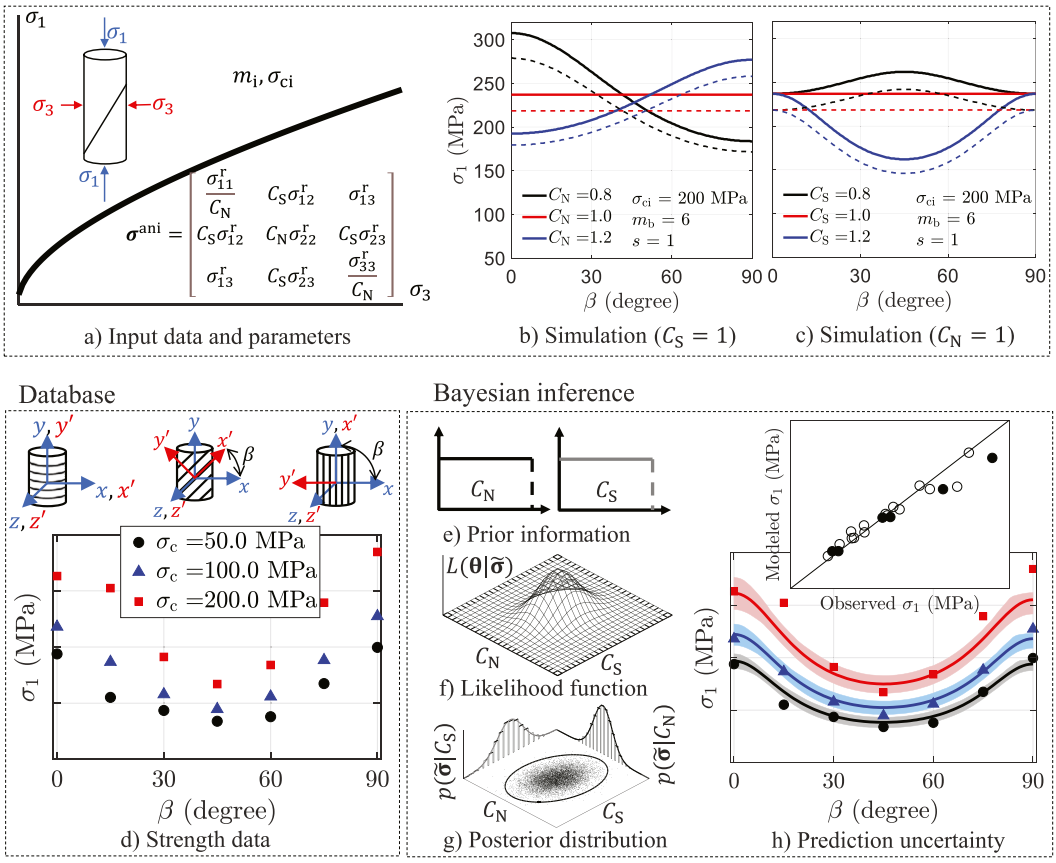

Fig. 1. Schematic overview of the different building blocks of our uncertainty-based framework for rock strength anisotropy. The top panel illustrates the modeling steps including isotropic Hoek–Brown constants and the introduced anisotropic parameters (a), and sensitivity of the model to the values of the scaling factors C_N (b) and C_S (c) when rotating the anisotropy direction for confining stresses of σ_c = 10 MPa (solid lines) and σ_c = 5 MPa (dashed lines). The bottom panel exemplifies the database used in this research (left) and the main parts of the Bayesian analysis (right) for the inference of the anisotropic model parameters. (For interpretation of the references to color in this figure legend, the reader is referred to the web version of this article.)

2. Methodology

Our uncertainty quantification framework of rock strength anisotropy is comprised of three building blocks, including our HB numerical model of rock anisotropy, a database of experimental data and a general-purpose method for Bayesian analysis of the anisotropic HB model parameters. Fig. 1 provides a schematic overview of the proposed methodology. The top panel provides a brief description of our numerical model, including (a) definition of the isotropic HB constants and anisotropic parameters and a simple demonstration of the model sensitivity to the values of the dimensionless scaling factors (b) C_N and (c) C_S when rotating the direction of anisotropy, using confining stress, σ_c, of 10 MPa (solid lines) and 5 MPa (dashed lines). The panel in the left bottom, labeled (d), constitutes the experimental data that are used for HB model training and evaluation. Finally, the panel in the right bottom summarizes the main elements of our Bayesian framework. This panel provides a graphical illustration of the bivariate (e) prior distribution, (f) likelihood function and (g) posterior distribution of the anisotropic HB model parameters, C_N and C_S. Fig. 1 also presents a scatter plot of the observed and simulated rock strengths, including and the 95% prediction intervals due to parameter (dark region) and model (light region) uncertainty. The next subsections detail the different steps of the graphical illustration presented in Fig. 1.

2.1. Model description

The isotropic HB strength criterion[11] considers the nonlinear relationship between the major, σ_1 ($ML^{-1}T^{-2}$), and minor, σ_3 ($ML^{-1}T^{-2}$), effective principal stresses under the ultimate failure state (Fig. 1a), as follows[44]:

$$\sigma_1 = \sigma_3 + \sigma_{ci}\left(m_i \frac{\sigma_3}{\sigma_{ci}} + s\right)^a, \tag{1}$$

where σ_{ci} ($ML^{-1}T^{-2}$) denotes the uniaxial compressive strength of the intact rock, m_i is a unitless material constant for intact rock, and s and a are dimensionless parameters that reflect the characteristics of the rock mass. For intact rocks, $s = 1$ and $a = 0.5$. Ref. 13 have shown that the material constant, m_i, is a rock characteristic independent of the loading direction.

If we use F ($ML^{-1}T^{-2}$) as our failure criterion, then Eq. (1) can be written as:

$$F = \sigma_1 - \sigma_3 - \sigma_{ci}\left(m_i \frac{\sigma_1}{\sigma_{ci}} + s\right)^a = 0. \tag{2}$$

To account for anisotropy in the HB empirical formulation, we express Eq. (2) in terms of the stress tensor, $\boldsymbol{\sigma}$ ($ML^{-1}T^{-2}$), invariants:

$$F = \sigma_{ci}\left[\frac{\sqrt{J_2}(2\cos\theta)}{\sigma_{ci}}\right]^{1/a} + \sqrt{J_2}m_i\left(\cos\theta + \frac{1}{\sqrt{3}}\sin\theta\right) - \frac{m_b I_1}{3} - \sigma_{ci}s, \tag{3}$$

where I_1 ($ML^{-1}T^{-2}$) signifies the first invariant of the stress tensor, J_2 ($M^2L^{-2}T^{-4}$), denotes the second invariant of the deviatoric stress tensor, $\boldsymbol{\sigma}'$ ($ML^{-1}T^{-2}$), and θ (°) is the Lode angle. These scalar quantities of the stress tensor are defined below:

$$I_1 = \sigma_m = \sigma_1 + \sigma_2 + \sigma_3, \tag{4}$$

$$J_2 = \frac{1}{2}\sigma_{ij}\sigma_{ji}, \tag{5}$$

$$\theta = -\frac{1}{3}\arcsin\left[\frac{3\sqrt{3}}{2}\left(\frac{J_3}{J_2}\right)^3\right] \quad \text{for} -\pi/6 \le \theta \le \pi/6, \tag{6}$$

where σ_2 ($ML^{-1}T^{-2}$) is the intermediate effective principal stress, and J_3 represents the third invariant of the deviatoric stress tensor. One can show that this third invariant equals the determinant of $\boldsymbol{\sigma}'$.[75]

Our anisotropic formulation uses as main building block the isotropic HB strength criterion[11] as detailed above. Yet, this isotropic strength criterion cannot characterize strength anisotropy in rocks. We follow the elastoplastic models of Mánica et al.[71] and Forero et al.[70] and formulate an anisotropic strength criterion with the help of the unitless scalar orientation parameters, C_N and C_S. As the strength of anisotropic rocks depends on how the loading is applied relative to the orientation of their anisotropy planes, this approach provides a simple way to relate the loading direction to the anisotropy direction. Fig. 1d illustrates our definition of the axis of anisotropy and the angle, β (°), between the anisotropy plane and the horizontal plane. This angle, β, may be designated as the "orientation angle". The global (x-y-z) and local (x'-y'-z') coordinate systems are also shown. The angle, β, is oriented counterclockwise from the horizontal and may represent the direction of the potential shear plane. As highlighted in Fig. 1d, the anisotropy plane, $\beta = 0°$, is perpendicular to the axial (vertical) axis (direction of the maximum applied load to the sample). Accordingly, $\beta = 45°$ for an inclined anisotropic plane and $\beta = 90°$ for a plane parallel to the axial axis.

The stress tensor, $\boldsymbol{\sigma}$, of the global coordinate system can be transformed into the local coordinate system, $\boldsymbol{\sigma}^r$, using the 3 × 3 rotation matrix, $\mathbf{R}$, as follows:

$$\boldsymbol{\sigma}^r = \mathbf{R}\boldsymbol{\sigma}\mathbf{R}^\top. \tag{7}$$

where $\top$ denotes transpose. The rotation matrix, $\mathbf{R}$, is comprised of the following entries:

$$\mathbf{R} = \begin{bmatrix} \cos\beta\cos\alpha_r & \sin\beta & -\cos\beta\sin\alpha_r \\ -\cos\alpha_r\sin\beta & \cos\beta & \sin\beta\sin\alpha_r \\ \sin\alpha_r & 0 & \cos\alpha_r \end{bmatrix}, \tag{8}$$

where α_r (°) is defined as the angle of rotation of the y axis. We follow Ref. 70 and set $\alpha_r = 0$, thus, assuming no rotation of the y axis. Furthermore, the anisotropic stress tensor, $\boldsymbol{\sigma}^{ani}$, is defined as in Ref. 71 using a non-uniform scaling of the stress tensor oriented with the local coordinate system $\boldsymbol{\sigma}^r$:

$$\boldsymbol{\sigma}^{ani} = \begin{bmatrix} \frac{\sigma^r_{11}}{C_N} & C_S\sigma^r_{12} & \sigma^r_{13} \\ C_S\sigma^r_{12} & C_N\sigma^r_{22} & C_S\sigma^r_{23} \\ \sigma^r_{13} & C_S\sigma^r_{23} & \frac{\sigma^r_{33}}{C_N} \end{bmatrix}, \tag{9}$$

where σ^r_{ij} denotes the (i,j)th stress component of the local coordinate system and C_N and C_S, signify the normal and shear scaling factors, respectively. The effect of the anisotropic parameters, C_N and C_S, have on the rock strength in our new anisotropic formulation, is illustrated in Fig. 1(b and c). In summary, the anisotropic HB formulation as proposed herein can simulate the strength of anisotropic rocks for different loading directions and magnitudes of the confining stress, σ_c. For unit values of the scaling factors C_N and C_S, our anisotropic model formulation simplifies to the isotropic HB failure criterion, independently of the orientation angle, β. A detailed analysis on how the dimensionless scaling factors, C_N and C_S affect the rock strength when rotating the anisotropy direction is presented in Refs. 70, 71, and, thus, will not be repeated herein.

Now, the mathematical formulation of our anisotropic HB strength criterion has been completed, we are left with its computational implementation. In doing so, we resort to a hydrostatic stress state and set the effective principal stresses equal to the confining stress, σ_c. Then, the major principal stress σ_1 is changed in incremental steps to satisfy Eq. (2). Altogether, our anisotropic HB strength criterion has six input arguments, including two forcing variables, β and σ_c, and four parameters, m_b, σ_{ci}, C_N and C_S. Table 1 provides a brief description of these different variables, including their units and prior (feasible) ranges. The isotropic HB parameters, m_b and σ_{ci}, were held fixed for each anisotropic rock investigated in this study, details of which will be discussed in the next subsection.

Table 1
Forcing variables, isotropic and anisotropic parameters of the anisotropic HB strength criterion.

Model component	Symbol	Description	Unit	Ranges
Forcing variable	β	Orientation angle	°	0–90
Forcing variable	σ_c	Confining stress	MPa	0–200
Isotropic parameter	m_i	Constant for the intact rock	–	1–30
Isotropic parameter	σ_{ci}	Uniaxial compressive strength	MPa	60–225
Anisotropic parameter	C_N	Normal scaling factor	–	0.5–1.5
Anisotropic parameter	C_S	Shear scaling factor	–	0.5–2.5

Algorithm 1 presents a step-by-step recipe on how to compute the peak strength, σ_1, using the anisotropic HB strength criterion. The basic idea of the proposed procedure is to increase the major principal stress with an increment, $\Delta\sigma_1$, until F is equal or lower than a small convergence threshold, err. Although we used in our study only increments of σ_1, we note here that σ_2 could also be incremented by modifying the stress tensor, as performed in line 13 for σ_1. This could provide a basis to account for the influence of the intermediate principal stress. The convergence threshold, err, and increment, $\Delta\sigma_1$, exert a strong control on the efficiency of Algorithm 1. If the values of err and/or $\Delta\sigma_1$ are set too small then it may take a prohibitively large number of iterations to solve for the peak strength, σ_1, as a function of confining stress, σ_c, and orientation angle, β. Preliminary analysis has demonstrated that the values of err = 3 and $\Delta\sigma_1 = 0.5$ work well for the data sets considered herein. These values provided an adequate trade-off between the computational efficiency of the algorithm and the accuracy of the inferred peak strengths. The use of smaller values of err and $\Delta\sigma_1$ considerably deteriorates the CPU-efficiency of the algorithm without changing much the final estimates of the peak strength. The formulation as proposed in this paper is relatively simple to implement and has an additional advantage since our approach does not use complex components of elastoplastic models as in previous studies.[70,71]

Algorithm 1 Anisotropic HB strength criterion with scaled stress tensor

1: Define model parameters $m_b, \sigma_{ci}, C_N, C_S$
2: Define forcing variables σ_c, β
3: Compute the hydrostatic stress tensor, $\boldsymbol{\sigma}$, in the global system
4: Initialize F with a large value
5: **while** $|F| >$ err **do**
6: Compute the stress rotation matrix, $\boldsymbol{\sigma}^r$, using Equation (7)
7: Compute the anisotropic stress tensor, $\boldsymbol{\sigma}^{ani}$, using Equation (9)
8: Compute stress invariants I_1, J_2, and θ using Eqs. (4), (5), (6), respectively
9: Compute the failure criterion, F, using Equation (3)
10: **if** $|F| \le$ err **then**
11: return the peak strength, σ_1
12: **else**
13: $\sigma_1 \leftarrow \sigma_1 + \Delta\sigma_1$
14: **return** σ_1 ▷ σ_1 is the peak strength

2.2. Database

Experimental data were collected from different, well-known, literature studies (Table 2). A total of eight anisotropic rocks was analyzed, specifically, (1) Green river shale,[8] (2) gneiss,[9] (3) Moretown phyllite,[76] (4) Penrhyn slate,[10] (5) slate,[11] (6) Tournemire shale,[12] (7) Mancos shale,[14] and (8) gneiss A.[13] In each cited publication, the

Table 2
Overview of the different anisotropic rocks used in our analysis, including type, literature reference of the data set, the corresponding values of the HB parameters, σ_{ci} and m_i, for intact rock, measured values of the minimum and maximum peak strength (MPa) and prior ranges of the anisotropic parameters, C_N and C_S, used in our analysis. The last column quantifies the strength of the correlation between the bivariate posterior samples of the scaling factors, C_N and C_S. This column will be addressed in the discussion section.

Rock type	Reference	HB parameters		Peak strength		C_N		C_S		ρ
		σ_{ci}	m_i	min.	max.	min.	max.	min.	max.	
1. Green river shale II	Ref. 8	106.0	4.9	95.1	356.2	0.5	1.5	0.5	2.0	0.02
2. Gneiss	Ref. 9	215.0	28.5	141.1	553.3	0.5	1.5	0.5	1.2	−0.09
3. Moretown phyllite	Ref. 76	247.0	6.90	135.9	738.3	0.5	1.5	0.5	2.0	0.06
4. Penrhyn slate	Ref. 10	206.6	6.2	39.0	471.3	0.5	1.5	0.5	2.5	−0.06
5. Slate	Ref. 11	225.0	4.7	152.3	821.3	0.5	1.5	0.5	2.5	0.09
6. Tournemire shale[a]	Ref. 12	74.0	1.0	57.7	111.8	0.5	1.5	0.5	2.0	0.11
7. Mancos shale[a]	Ref. 14	62.4	8.1	39.3	65.0	0.5	1.5	0.5	2.0	−0.01
8. Gneiss A	Ref. 13	60.6	27.8	37.2	269.7	0.5	1.5	0.5	1.4	−0.12

[a]Isotropic HB model parameters determined using the *RocLab* software package.

authors carried out extensive laboratory experiments and the resulting eight data sets have in common the measurement of mechanical rock properties for different confining stresses, σ_c, and orientation angles, β. This is particularly important, as σ_c and β exert a large control on the strength of anisotropic rocks.

For intact rock, the values of the material constants, s and a, are set to 1 and 0.5, respectively. The values of the isotropic HB model parameters (intact rock), σ_{ci} and m_i, for (1) Green river shale II, (2) gneiss, (3) Moretown phyllite, (4) Penrhyn slate and (8) gneiss A, were obtained from Ref. 49 and their values for (5) slate originate from Ref. 11. For the remaining two anisotropic rocks, (6) Tournemire shale[12] and (7) Mancos shale[14], the isotropic HB (intact rock) model parameters, σ_{ci} and m_i, were determined using the Levenberg–Marquardt algorithm implemented within the *RocLab* software package[35,77]. These isotropic parameters can be determined by means of inverse modeling of peak strength data at $\beta = 0°$. Table 2 summarizes key variables of the experimental data of the eight anisotropic rock types. Specifically, for each rock type, we provide a data reference, report the values of σ_{ci} and m_i for intact rock, list the minimum and maximum measured peak strengths and document the ranges of the scaling factors, C_N and C_S, used in our analysis. The last column lists the correlation coefficient between the posterior samples of C_N and C_S. We will revisit this last column in our discussion section. For the time being, we conclude that the two scaling factors of our anisotropic HB formulation are uncorrelated for all different rock types. This is an important finding, which inspires confidence in the formulation of our anisotropic HB model, a claim that will be backed up by further evidence in the results section. Note that the strength values encompass a large range of rock failures, from 37 MPa to 821 MPa. For all rock types, the peak strength reported in Table 2 is evaluated in terms of the major principal stress, σ_1. Exceptions are made for the (6) Tournemire shale and (7) Mancos shales, where the peak strengths were evaluated in terms of the deviatoric stress, σ_d, and unconfined compressive strength (UCS), respectively. Lastly, the investigated rocks exhibit different degrees of anisotropy, from "low to medium" in shales and gneisses to "medium to very high" in slates and phyllite[1].

2.3. Bayesian inference

The Bayesian paradigm offers a coherent and integrated framework for systematically addressing different sources of modeling uncertainty in statistical inference of state variables, model inputs and/or parameters, nuisance and latent variables. This methodology has received much attention in the past two decades made possible, in large part, by continued advances in computational speed and power, and a growing recognition by researchers and/or decision makers that modeling results should be accompanied by estimates of uncertainty. Indeed, much progress has been made in the application of Bayesian analysis for reconciling dynamic system models with data.[74] For example, in geotechnical engineering, there is a steadily growing body of literature on the application of Bayesian analysis to inverse modeling and quantification of model parameter and output uncertainty.[51,55–58,60,70]

Bayesian inference allows for an exact description of parameter uncertainty by treating the parameters (and nuisance variables) as probabilistic variables with joint posterior probability density function, $p(\boldsymbol{\theta}|\tilde{\boldsymbol{\sigma}}_1)$. This multivariate distribution, the so-called posterior parameter distribution, is the consequence of two antecedents, a prior distribution, $p(\boldsymbol{\theta})$, which captures our initial degree of beliefs in the values of the model parameters, $\boldsymbol{\theta}$, and a likelihood function, $L(\boldsymbol{\theta}|\tilde{\boldsymbol{\sigma}}_1)$, which quantifies, by the rules of probability theory, the level of confidence (= conditional belief) in the parameter values in light of the observed peak strength data, $\tilde{\boldsymbol{\sigma}}_1 = (\tilde{\sigma}_{1,1}, \tilde{\sigma}_{1,2}, \dots, \tilde{\sigma}_{1,n})$, where the subscripts of $\tilde{\sigma}_{1,2}$ refer to sample 2 of the peak strength $\tilde{\sigma}_1$, etc.

Bayes' theorem can be derived from the basic axioms of probability, specifically conditional probability, and reads in our application

$$p(\boldsymbol{\theta}|\tilde{\boldsymbol{\sigma}}_1) = \frac{p(\boldsymbol{\theta})L(\boldsymbol{\theta}|\tilde{\boldsymbol{\sigma}}_1)}{p(\tilde{\boldsymbol{\sigma}}_1)} \propto p(\boldsymbol{\theta})L(\boldsymbol{\theta}|\tilde{\boldsymbol{\sigma}}_1), \tag{10}$$

where the denominator, $p(\tilde{\boldsymbol{\sigma}}_1)$, the so-called evidence or marginal likelihood, acts as a normalizing constant

$$p(\tilde{\boldsymbol{\sigma}}_1) = \int_{\boldsymbol{\Theta}} p(\boldsymbol{\theta})P(\tilde{\boldsymbol{\sigma}}_1|\boldsymbol{\theta})\mathrm{d}\boldsymbol{\theta} = \int_{\boldsymbol{\Theta}} P(\boldsymbol{\theta})L(\boldsymbol{\theta}|\tilde{\boldsymbol{\sigma}}_1)\mathrm{d}\boldsymbol{\theta} = \int_{\boldsymbol{\Theta}} p(\boldsymbol{\theta}|\tilde{\boldsymbol{\sigma}}_1)\mathrm{d}\boldsymbol{\theta}, \tag{11}$$

so that the posterior distribution, $p(\boldsymbol{\theta}|\tilde{\boldsymbol{\sigma}}_1)$, integrates to unity over the prior (feasible) parameter space, $\boldsymbol{\theta} \in \boldsymbol{\Theta} \subseteq \mathbb{R}^d$. Knowledge of $p(\tilde{\boldsymbol{\sigma}}_1)$ is strictly necessary for hypothesis testing to select the most plausible model from a set of different candidate models deemed valid apriori. For now, we suffice to say that the evidence of a model is largest, if its data likelihood, $L(\boldsymbol{\theta}|\tilde{\boldsymbol{\sigma}}_1)$, is high relative to other candidate models and distributed uniformly over its prior parameter space, $\boldsymbol{\Theta}$. As our focus is on statistical inference of the scaling factors, C_N and C_S, using the measured peak strength data, $\tilde{\boldsymbol{\sigma}}_1$, we can ignore the evidence, $p(\tilde{\boldsymbol{\sigma}}_1)$, without harm and work instead with the unnormalized posterior distribution as articulated by the proportionality sign in Eq. (10). We refer to Ref. 74 and references therein for a review of Bayesian analysis and its application to various fields.

In our case, $\boldsymbol{\theta}$, is synonymous to the parameters, C_N and C_S, of our anisotropic HB strength criterion, hence, $\boldsymbol{\theta} = (C_N, C_S)$ and $\tilde{\boldsymbol{\sigma}}_1$ signifies the n-vector of peak strength measurements for each anisotropic rock considered herein. In the next subsections, we will detail our choice of prior distribution, $p(\boldsymbol{\theta})$, for the anisotropic parameters and present our formulation of the likelihood function, $L(\boldsymbol{\theta}|\tilde{\boldsymbol{\sigma}}_1)$, in pursuit of the posterior probability distribution, $p(\tilde{\boldsymbol{\sigma}}_1|\boldsymbol{\theta})$, of C_N and C_S, respectively. Furthermore, we will briefly discuss the methodology (software package) used to derive the posterior parameter distribution.

2.3.1. Prior distribution of the anisotropic model parameters

The prior distribution, $p(\boldsymbol{\theta})$, should encode all the "subjective" knowledge about the scaling factors, $\boldsymbol{\theta} = (C_N, C_S)$, before collection of the peak strength data, $\tilde{\boldsymbol{\sigma}}_1$. This distribution, often simply called

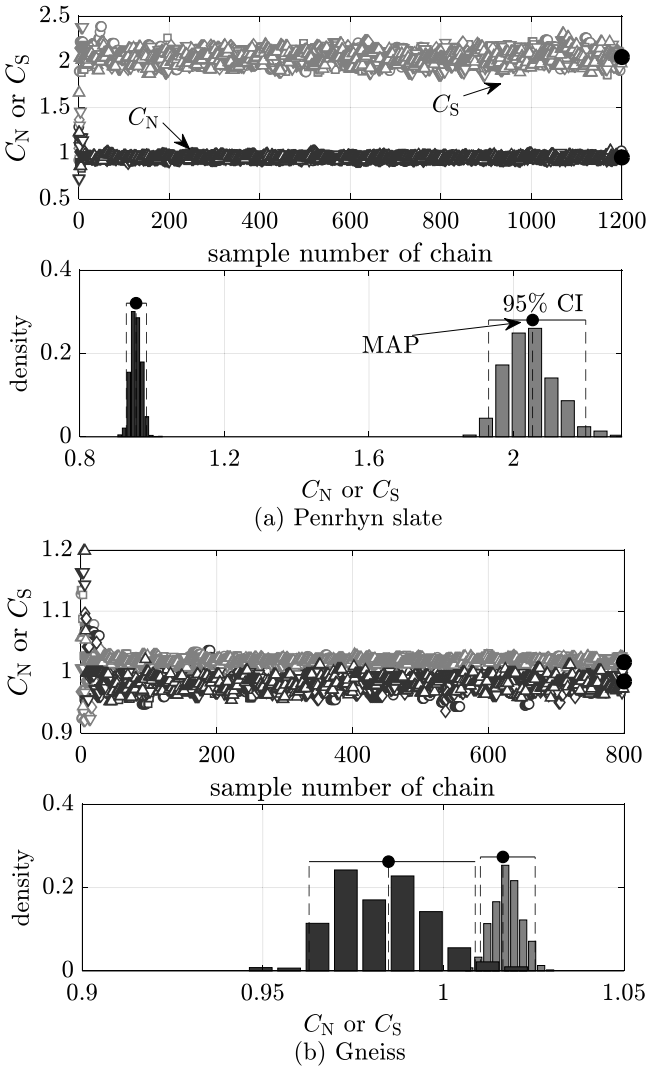

Fig. 2. Trace plots (top) and histograms of the posterior distributions (bottom) of C_N (dark gray) and C_S (light gray) fitted to the collected dataset for the (4) Penrhyn slate (a) and (2) gneiss (b). The MAP (solid black point) and the 95% confidence intervals (CI) of the parameters are also indicated.

the prior, expresses one's beliefs about the parameters before the peak strength data (also referred to as evidence) are taken into account. In the absence of detailed information about the values of the anisotropic model parameters, we assign a noninformative prior distribution to C_N and C_S using the ranges stipulated in Table 2. This choice of $d = 2$-dimensional hypercube is synonymous to a bivariate uniform prior distribution (see Fig. 1e) with scaling factors for (7) Tournemire shale equal to $0.5 \leq C_N \leq 1.5$ and $0.5 \leq C_S \leq 2.0$ and density on the vertical or z-axis, $p(\boldsymbol{\theta}) = 1/\big((1.5-0.5)\times(2.0-0.5)\big) = \frac{2}{3}$, so that the prior distribution integrates to one. Based on preliminary runs of our anisotropic HB model, the minimum value of each scaling factor was set to 0.5, whereas the maximum value of C_N was fixed at 1.5 and the upper bound of C_S was made dependent on rock type. These so-called prior ranges of the two anisotropic model parameters may appear somewhat conservative, nevertheless, allows simulation of a wide variety of shapes of the (σ_1, β) relationship depicted graphically in our methodological overview in Figs. 1b and c. The general-purpose sampling method used herein has a demonstrated efficacy and efficiency on a large suite of test problems and applications, hence, will not suffer from a more dispersed prior distribution of C_N and C_S. Care should always be exercised that the prior distribution is wide enough to not discard feasible solutions of the two scaling factors and truncate their bivariate and marginal posterior distributions.

An uninformative prior does not favor apriori any values of the anisotropic model parameters, C_N and C_S, rather lets the peak strength data, $\widetilde{\boldsymbol{\sigma}}_1 = (\widetilde{\sigma}_{1,1}, \widetilde{\sigma}_{1,2}, \ldots, \widetilde{\sigma}_{1,n})$, speak for itself. This implies that the posterior density, $p(\boldsymbol{\theta}|\widetilde{\boldsymbol{\sigma}}_1)$, of the anisotropic HB model parameters, C_N and C_S, is simply equal to a fixed multiple of two-thirds of the likelihood, $L(\boldsymbol{\theta}|\widetilde{\boldsymbol{\sigma}}_1)$, for all $\boldsymbol{\theta} \in \boldsymbol{\Theta}$. As a result, the scaling factors, C_N and C_S, which maximize the posterior density, $p(\boldsymbol{\theta}|\widetilde{\boldsymbol{\sigma}}_1)$, are synonymous with maximum likelihood estimates.

2.3.2. Choice of likelihood function

The likelihood was designated as a mathematical quantity by Sir Ronald Fisher[78] to measure our degree of belief (confidence) in simulated outcomes. In this application, the likelihood (function) quantifies in probabilistic terms the distance between the observed, $\widetilde{\boldsymbol{\sigma}}_1$, and simulated, $\boldsymbol{\sigma}_1$, peak strength data using our formulation of the anisotropic HB model and the scaling factors, $\boldsymbol{\theta} = (C_N, C_S)$.

If we make the common and convenient assumption that the measurement errors of the peak strength observations follow a zero-mean normal distribution with a constant variance, $\sigma^2_{\widetilde{\sigma}}$, then the likelihood function becomes

$$L(\boldsymbol{\theta}|\widetilde{\boldsymbol{\sigma}}_1, \sigma^2_{\widetilde{\sigma}}) = \prod_{i=1}^{n} \frac{1}{\sqrt{2\pi\sigma^2_{\widetilde{\sigma}}}} \exp\left[-\frac{1}{2}\left(\frac{\widetilde{\sigma}_{1,i} - \sigma_{1,i}(\boldsymbol{\theta})}{\sigma_{\widetilde{\sigma}}}\right)^2\right], \tag{12}$$

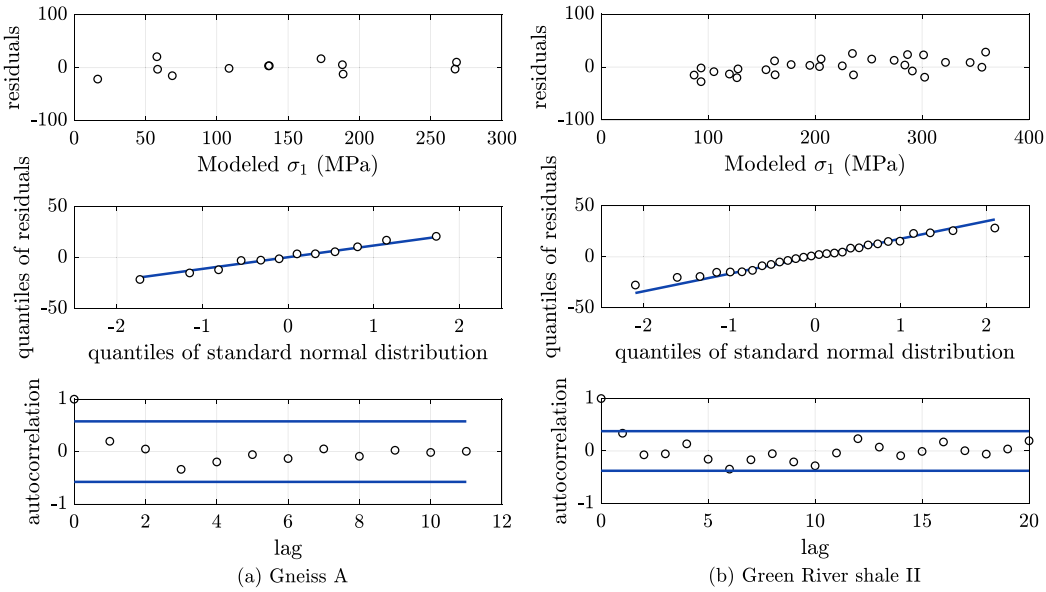

Fig. 3. Diagnostic tests of the model residuals using rock strength data for the (8) gneiss A (a) and (1) Green river shale II (b): residuals as a function of the modeled peak stress (top), quantile–quantile plots (middle), and autocorrelation function with theoretical 95% significance intervals of strength data of uncorrelated residuals (bottom).

where the difference, $\widetilde{\sigma}_{1,i} - \sigma_{1,i}(\boldsymbol{\theta})$, between the ith observed and simulated rock strength is the so-called residual

$$\mathbf{e}(\boldsymbol{\theta}) = \big(e_1(\boldsymbol{\theta}), e_2(\boldsymbol{\theta}), \dots, e_n(\boldsymbol{\theta})\big) = \widetilde{\boldsymbol{\sigma}}_1 - \boldsymbol{\sigma}_1. \tag{13}$$

The likelihood function of Eq. (12) can suffer from arithmetic underflow, that is, finite multiplication can result in a number that is very close to zero that the computer cannot store this in memory. This can already happen for relatively small n, say $n = 500$, particularly if the model poorly describes the observed data, and the residuals are large compared to the measurement error standard deviation, $|e_i(\boldsymbol{\theta}) \gg \sigma_{\widetilde{\sigma}}|$ for many elements $i \in (1, 2, \dots, n)$. For reasons of numerical stability it is therefore convenient to work with the log-likelihood, $\mathcal{L}(\boldsymbol{\theta}|\widetilde{\boldsymbol{\sigma}}_1, \sigma^2_{\tilde{\mathbf{y}}})$, instead

$$\mathcal{L}(\boldsymbol{\theta}|\widetilde{\boldsymbol{\sigma}}_1, \sigma^2_{\widetilde{\sigma}}) = -\frac{n}{2}\log(2\pi) - \frac{n}{2}\log(\sigma^2_{\widetilde{\sigma}}) - \frac{1}{2}\sigma^{-2}_{\widetilde{\sigma}}\sum_{i=1}^{n}\big(\widetilde{\sigma}_{1,i} - \sigma_{1,i}(\boldsymbol{\theta})\big)^2. \tag{14}$$

This log-likelihood formulation is arguably also easier to interpret algebraically. The measurement error variance of the peak strength data, $\sigma^2_{\widetilde{\sigma}}$, can be defined by the user, its value can be inferred simultaneously with the parameters, $\boldsymbol{\theta}$, or be integrated out of Eq. (16). If the variance of the residuals,

$$s^2 = \frac{1}{n-1}\sum_{i=1}^{n}\big(e_i(\boldsymbol{\theta})\big)^2, \tag{15}$$

is taken as sufficient statistic for $\sigma^2_{\widetilde{\sigma}}$, then the log-likelihood function, $\mathcal{L}(\boldsymbol{\theta}|\widetilde{\boldsymbol{\sigma}}_1, \sigma^2_{\widetilde{\sigma}})$, simplifies to Ref. 74

$$\mathcal{L}(\boldsymbol{\theta}|\widetilde{\boldsymbol{\sigma}}_1) \propto -\frac{n}{2}\log\left(\sum_{i=1}^{n}\big(\widetilde{\sigma}_{1,i} - \sigma_{1,i}(\boldsymbol{\theta})\big)^2\right), \tag{16}$$

and the likelihood function, $L(\boldsymbol{\theta}|\widetilde{\boldsymbol{\sigma}}_1)$, equals

$$L(\boldsymbol{\theta}|\widetilde{\boldsymbol{\sigma}}_1) \propto \sum_{i=1}^{n}|\widetilde{\sigma}_{1,i} - \sigma_{1,i}(\boldsymbol{\theta})|^{-n}. \tag{17}$$

If we now apply Bayes theorem, $p(\boldsymbol{\theta}|\widetilde{\boldsymbol{\sigma}}_1) \propto p(\boldsymbol{\theta})L(\boldsymbol{\theta}|\widetilde{\boldsymbol{\sigma}}_1)$, in Eq. (10), then the posterior density is equivalent to

$$p(\boldsymbol{\theta}|\widetilde{\boldsymbol{\sigma}}_1) \propto \sum_{i=1}^{n}|\widetilde{\sigma}_{1,i} - \sigma_{1,i}(\boldsymbol{\theta})|^{-n}. \tag{18}$$

As is evident, the posterior density will find its maximum at the minimum of the sum of squared residuals. Thus, the least squares fit of our anisotropic HB model to the observed peak strength data will equal the maximum likelihood, and, thus, maximum a-posteriori (MAP) estimate of the scaling factors, C_N and C_S.

To verify that our assumptions of normality and independence of the peak strength measurement errors (residuals) are satisfied, we perform diagnostic checks of the n-vector of residuals, $\mathbf{e}(\boldsymbol{\theta}) = \big(e_1(\boldsymbol{\theta}), e_2(\boldsymbol{\theta}), \dots, e_n(\boldsymbol{\theta})\big)$. This approach includes tests for homoscedasticity, independence and normality of the residuals.

2.3.3. Posterior exploration

We infer the posterior distribution of the two scaling factors, C_N and C_S, in our anisotropic HB model using Markov chain Monte Carlo (MCMC) simulation with the DiffeRential Evolution Adaptive Metropolis (DREAM) software package.[72,73] This algorithm has shown an excellent performance in the sampling of complex posterior distributions, including high-dimensional and multi-modal target distributions.[74] In this work, we used the core of the DREAM algorithm released in a software publication.[74] Interested readers are referred to the cited publications for a detailed description of the DREAM algorithm. Several geotechnical applications of this method can be found in earlier publications.[55,57,60,70]

To evaluate the performance of the inferred scaling factors on an independent data set, we use split sampling and divide the n-vector of measured rock strengths of (2) gneiss, (3) Moretown phyllite, (4) Penrhyn slate and (5) slate, $\widetilde{\boldsymbol{\sigma}}_1 = (\widetilde{\sigma}_{1,1}, \widetilde{\sigma}_{1,2}, \dots, \widetilde{\sigma}_{1,n})$, into calibration and evaluation data set. In doing so, we randomly assign 75% of the observations to the training data set, and the remaining quarter of the peak strength measurements to an evaluation data set. To assess the robustness of our inference procedure and anisotropic HB model, we repeat this exercise 10 times. The length of the data set of the other four anisotropic rocks was insufficient for split sampling. Thus, for the (1) Green river shale II, (6) Tournemire shale, (7) Mancos shale and (8) gneiss A, all peak strength measurements were used for model training.

Two standard statistical metrics, the coefficient of determination (R^2) and the root mean squared error (RMSE), were used to analyze our results of the calibration and evaluation simulations.

3. Results and discussion

3.1. Posterior parameter uncertainty

Fig. 2 exemplifies trace plots (top) and histograms of the posterior distributions (bottom) of C_N and C_S derived from DREAM using 8

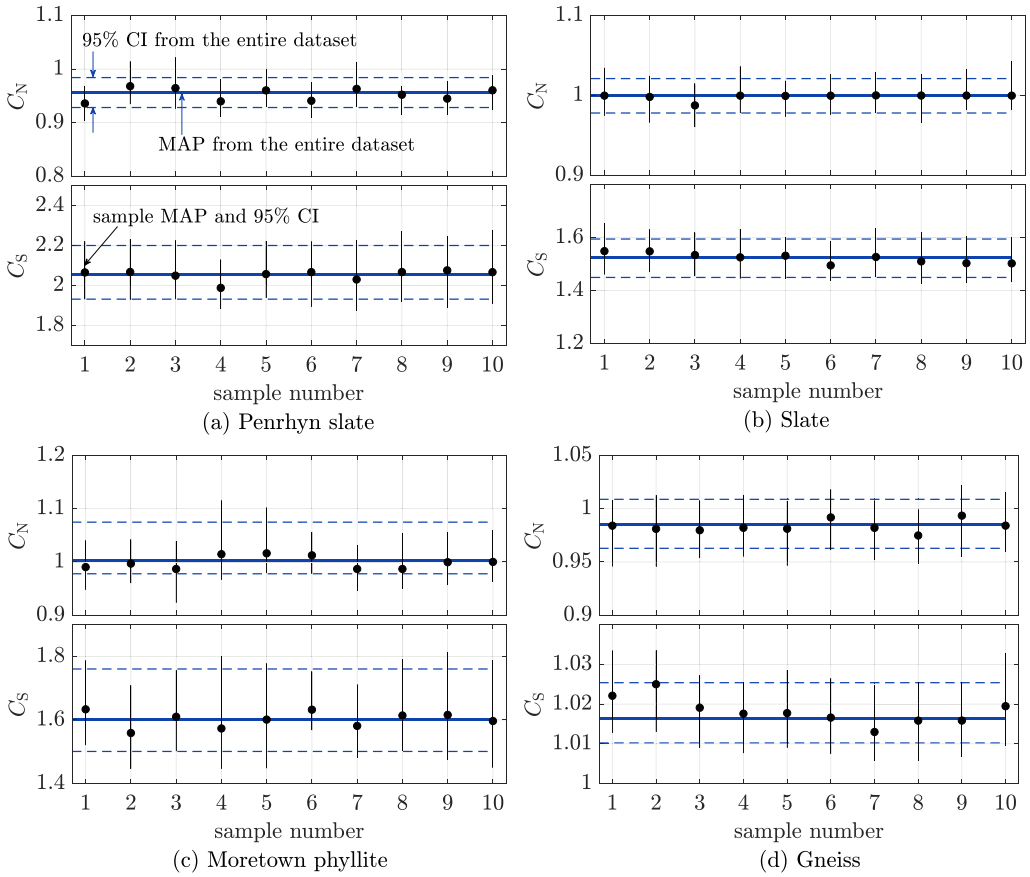

Fig. 4. Posterior estimates (MAP and 95% confidence intervals) for the anisotropic parameters, C_N and C_S, based on the full datasets (blue lines) and 10 randomly selected stress samples with 75% of the data for model calibration. The plots illustrate results for the (4) Penrhyn slate (a), (5) slate (b), (3) Moretown phyllite (c) and (2) gneiss (d).

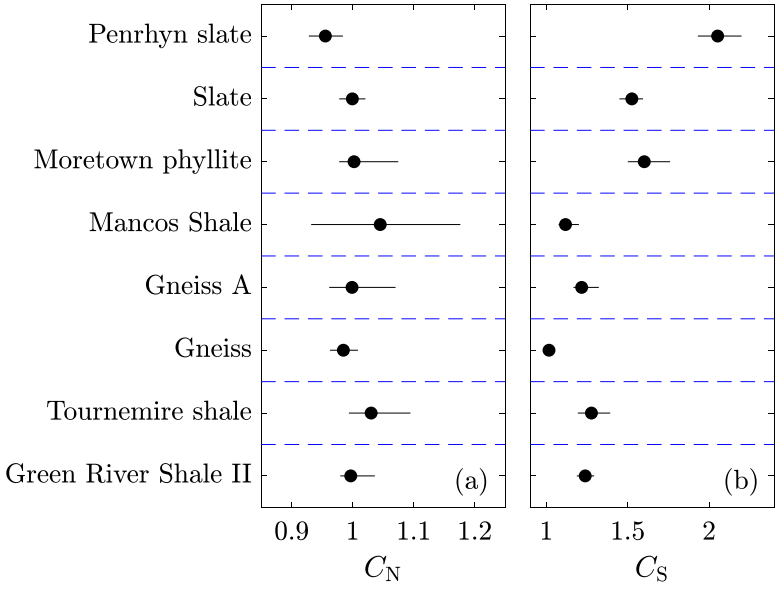

Fig. 5. Posterior parameter distributions for the anisotropic model parameters based on the full datasets. Black points represent the MAP solution for C_N (a) and C_S (b) while black lines illustrate the corresponding 95% uncertainty ranges of the parameter values.

Markov chains. Here, for brevity, we analyze only the posterior samples generated for the (4) Penrhyn slate (a) and (2) gneiss (b) using 1200 and 800 generations, respectively. This corresponds to 9600 (Penrhyn slate) and 6400 (gneiss) posterior samples generated with the DREAM algorithm. Individual chains are coded with different symbols. Dark gray symbols represent C_N samples, while light gray points depict C_S samples. The maximum a-posteriori (MAP) solution is separately indicated in each trace plot and histogram with a solid black point. These parameter values are associated with the highest value of the likelihood function of Eq. (17) of all posterior samples generated by DREAM, and this MAP solution coincides almost perfectly with the posterior median values. The 95% confidence intervals (CI) computed

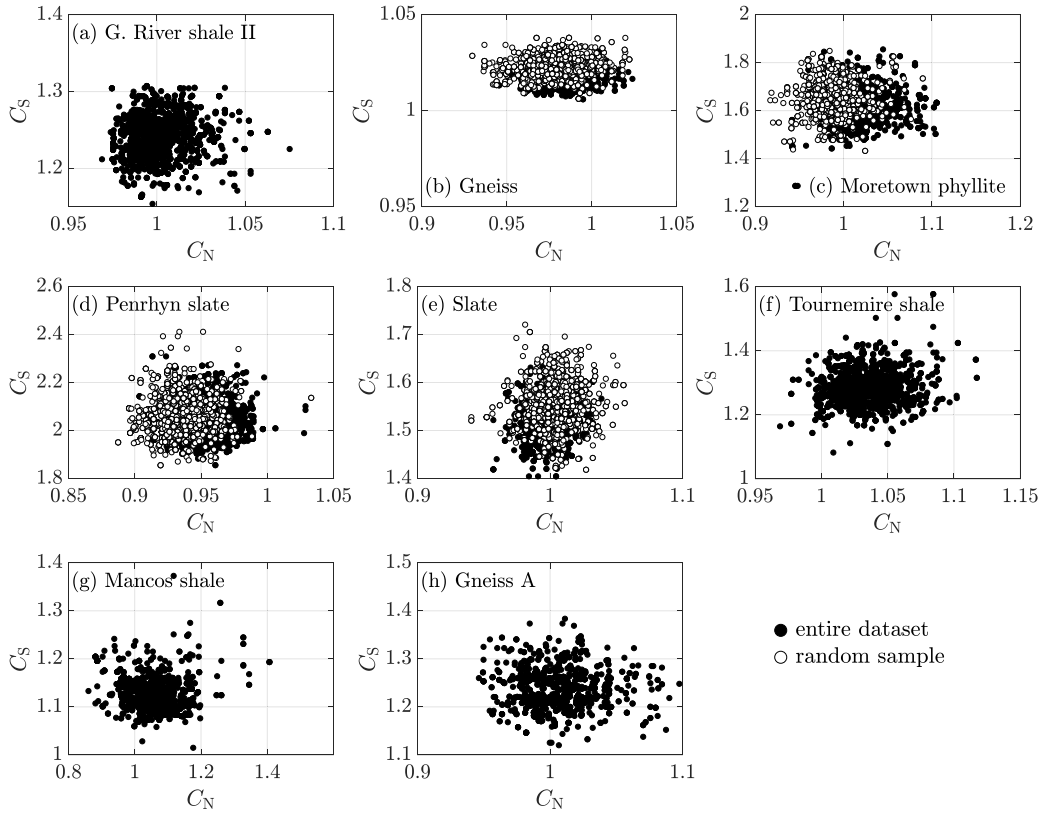

Fig. 6. Bivariate scatter plots of the posterior samples of C_N and C_S for the different investigated rocks. Filled and open circles represent correlation between the anisotropic parameters considering the full dataset and one random sample of the calibration data, respectively. The parameters exhibit a negligible correlation by calibration against the observed peak strength data.

from the posterior distributions of the parameters are also indicated in the plots.

Informal visual inspection of the sampled trace plots suggests convergence of all the chains (Fig. 2). Optionally, the DREAM algorithm has an arsenal of statistical measures to test whether the convergence to the posterior distribution has been achieved.[74] The posterior distributions of the last 25% of the samples stored in each of the 8 Markov chains demonstrates that both C_N and C_S are very well-defined by calibration against the observed rock strength data. In fact, the density histograms exhibit normality and occupy a small part of the prior distribution (see Table 2). Similar findings on the posterior parameter distributions of C_N and C_S have been reported by Forero et al.[70] using a modified version of the Lade–Kim constitutive model. Therefore, these posterior distributions can be further used for model simulation and prediction uncertainty. The MAP solution of C_S for the (4) Penrhyn slate near 2 indicates that this rock is highly anisotropic, with minimum strengths found when the major principal stress direction and the anisotropy plane has an intermediate angle, that is, between 30° and 60° (see blue curves in Fig. 1c). On the contrary, the posterior parameter distribution of C_S for the (2) gneiss assumes a different MAP value near 1, indicating that this investigated rock is weakly anisotropic and thus appears insensitive to parameter C_S if the material is oriented orthogonal, parallel or inclined to the loading direction. The remaining studied rocks have shown equivalent outcomes. We will revisit the parameter distributions of the random samples and all examined rocks latter.

The likelihood function adopted in this paper was based on assumptions of uncorrelated, homoscedastic, and normally distributed residuals. In Bayesian analysis, it is good practice to access if these assumptions are violated as the posterior distribution and the corresponding prediction uncertainty intervals might be subject to misinterpretation.[58,79,80] To assess the validity of these assumptions, Fig. 3 shows diagnostic tests of the residuals as a function of the peak stress, σ_1 (top), the quantile–quantile plot (middle) and the autocorrelation function (bottom) for the (8) gneiss A (a) and (1) Green river shale II (b). The top panel tests whether the magnitude of the residuals depends on the magnitude of the stress observations. The residuals seem homoscedastic, i.e., independent of the magnitude of the observed peak stress data. The middle panel presents a quantile–quantile plot that examines whether the residuals follow a normal distribution. Results show that the quantiles of the residuals were in good correspondence with this assumption for both anisotropic rocks. For these investigated rocks, the bottom panel shows that the autocorrelation at given lag (black circles) persisted within the theoretical 95% significance interval of residual stress levels (blue lines), demonstrating that the residuals are uncorrelated. Again, the remaining rocks under study have shown similar findings. We hence concluded that the assumptions of the likelihood model were satisfied and that parameter posterior distributions and equivalent prediction confidence intervals should be satisfactory.

Fig. 4 examines the MAP solution and the corresponding confidence intervals of C_N and C_S for rocks with a larger number of peak stress points, that is, (4) Penrhyn slate (a), (5) slate (b), (3) Moretown phyllite (c) and (2) gneiss (d). The plots indicate results obtained considering the full dataset and 10 different random samples, with 75% of the data for the model calibration. The results clearly indicate that the posterior estimates for both anisotropic parameters of the random samples (black lines) match closely the MAP (solid blue lines) and the 95% CI's (dashed blue lines) of the full dataset. This means that the samples analyzed with insufficient data might be considered as good estimates of the parameters of our anisotropic model. In fact, the random stress samples generate excellent estimates of C_N and C_S, in close agreement with calibration against the full datasets. Note that parameter C_N seems close to 1 for these rock samples, while C_S varies from 1 (weakly anisotropic

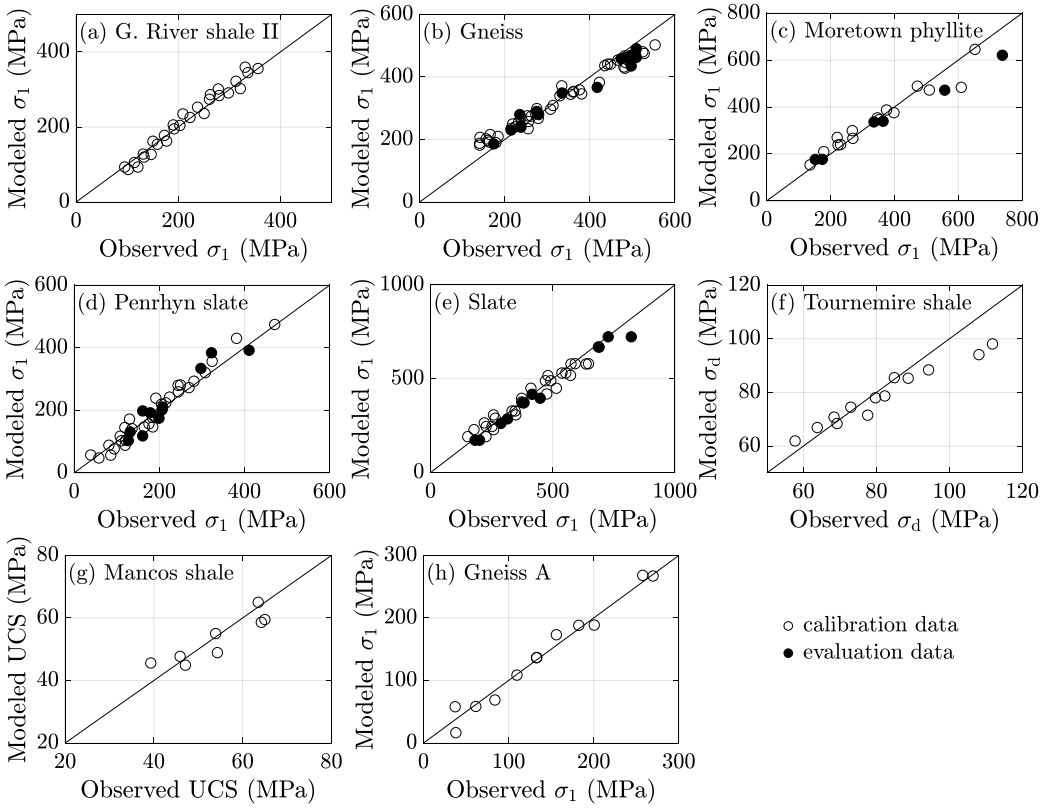

Fig. 7. Bivariate scatter plots that compare the observed and modeled rock strengths of the calibration (open circles) and randomly chosen evaluation (filled circles) datasets for all anisotropic rocks.

rocks) to 2 (highly anisotropic rocks). Although the posterior estimates displayed in Fig. 4 might reflect adequately the anisotropic parameter values of different rock types, we are left with the posterior estimates for all rock samples.

Based on the posterior parameter distributions derived with the DREAM algorithm, we now propose values for the anisotropic parameters of our model for all rock samples investigated (Fig. 5). Black points depict the MAP solution for C_N (a) and C_S (b), while black lines illustrate the corresponding 95% confidence intervals of the parameter values. An examination of the posterior MAP-values of C_N indicates that all values are close to one. This means that for rocks with minimum strengths found when the major principal stress direction and the anisotropy plane has an intermediate angle ($\beta = 30°$ to $\beta = 60°$), C_N-values near one are good estimates for this parameter. Thus, a more informative prior distribution can be further used to constrain the ranges of this parameter, particularly for cases when minimum strengths occur at an intermediate angle, β. Furthermore, the 95% uncertainty ranges for C_N are relatively small, except for the (7) Mancos shale. The large uncertainty of this last rock sample is related to the small number of peak strength observations (more of which later). These findings agree with results of Feng et al.,[58] which have indicated that the more *in situ* stress data implicates in more reliable stress estimates. However, as in engineering practice only limited strength data are available, estimates of the parameter uncertainty ranges are of paramount importance for geotechnical reliability analysis. In contrast to the similar values of C_N close to one, C_S-values are higher for highly anisotropic rocks, that is, (4) Penrhyn slate, (5) slate, and (3) Moretown phyllite, and lower for less anisotropic rocks. The 95% uncertainty ranges for C_S are also relatively small, suggesting that the model can adequately represent the strength behavior at intermediate orientations.

Altogether, the posterior histograms of the anisotropic model parameters centers nicely around their MAP solutions and follow an approximately normal distribution. The marginal distribution of the parameters occupies a small and defined portion of the uniform prior distribution, which demonstrates that both anisotropic parameters are very well-defined by calibration against the observed peak strength data. Moreover, the parameters exhibit negligible correlation by calibration against the observed peak strength data (Fig. 6). Indeed, C_N and C_S appear well calibrated with relatively tight uncertainty bounds, and small correlation among the individual parameters, which is confirmed by the correlation coefficients presented in Table 2. The derived correlation structures among posterior parameters do not vary with different studied rocks. This provides important insights into the uncertainty of the parameters C_N and C_S, indicating that our HB anisotropic model is efficient to model rock strength anisotropy. Now that the posterior MAP parameter values and the corresponding 95% confidence intervals derived from the calibration are estimated, we turn our attention to the performance of the proposed anisotropic HB model on the calibration and on the independent evaluation datasets.

3.2. Model simulation (prediction) uncertainty

Fig. 7 plots the observed versus modeled peak strength (σ_1) data for all the eight calibration cases. The solid black line is used to denote the identity or 1:1 line. The open circles in these regression plots represent calibration data, while the filled circles indicate evaluation data, randomly selected from one of the ten different samples. The modeled peak strengths agree well with laboratory observations for all rock samples. Note that the calibration and evaluation data for the (2) gneiss (b), (3) Moretown phyllite (c), (4) Penrhyn slate (d) and (5) slate (e) are similar, providing support for the claim that the proposed anisotropic model gives an adequate description of the rock strength using the split sampling technique. This is also supported by statistical analysis of the randomly chosen evaluation datasets (Fig. 8). R^2 and RMSE-values for the entire dataset are indicated by solid blue and red

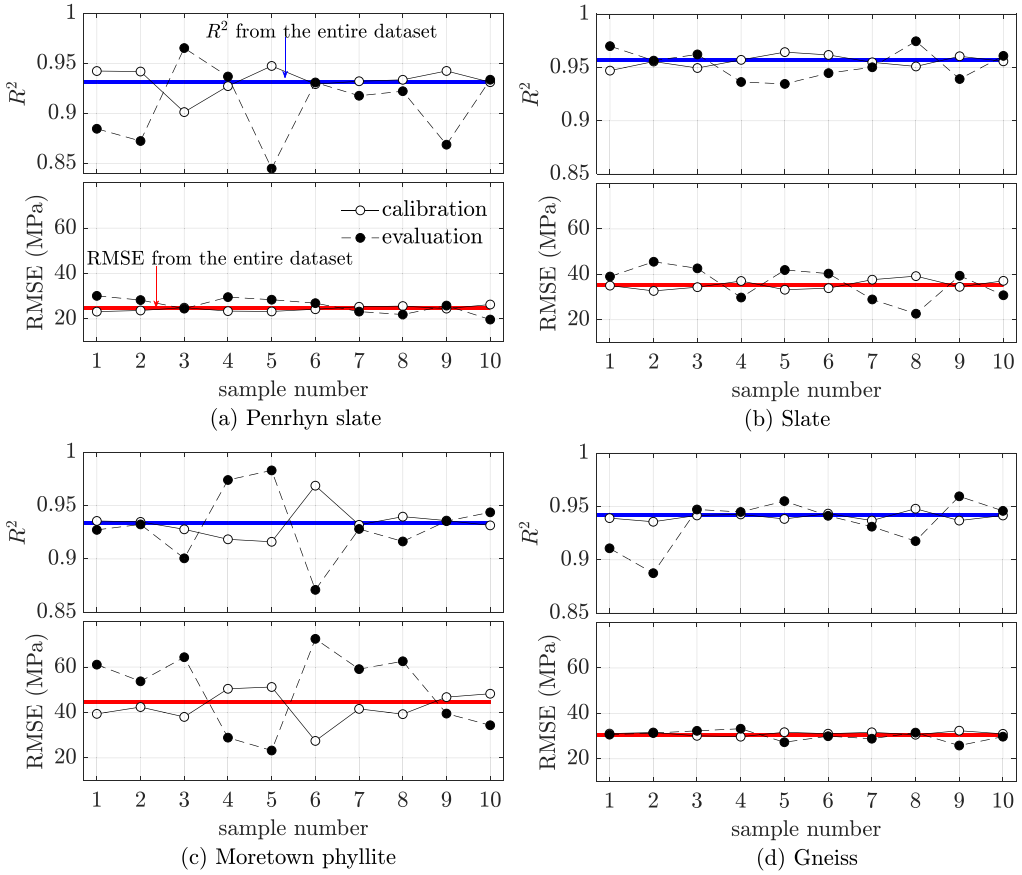

Fig. 8. Values of R^2 (blue solid lines) and RMSE (red solid lines) from the entire dataset for the (4) Penrhyn slate (a), (5) slate (b), (3) Moretown phyllite (c) and (2) gneiss (d). Dashed lines with open and filled circles represent different calibration and evaluation samples, respectively. (For interpretation of the references to color in this figure legend, the reader is referred to the web version of this article.)

lines in Fig. 8, respectively. Such values are in reasonable agreement with calibration and evaluation datasets of selected rocks. To simplify graphical interpretation, the statistical metrics share a common scale on the y axis. Note that R^2 near 0.95 for all rock samples demonstrate the general ability of the proposed model to describe accurately the strength of rocks with two anisotropic parameters. The different random samples exhibit similar values, with small variations around R^2-values of the entire dataset. Indeed, this is most noticeable for the (5) slate (b) and (2) gneiss (d). Larger differences between R^2-values of the entire dataset and the random samples are more appreciable for the (4) Penrhyn slate (a) and (3) Moretown phyllite (c). However, the R^2-values are higher than 0.85, demonstrating that our model produces reliable predictions outside the calibration domain. Similar conclusions can be made for the RMSE-values. Note that these RMSE results can be up to 60 MPa (e.g., (3) Moretown phyllite) and thus shall critically influence prediction uncertainty and reliability analysis.

We next analyze how uncertainty in the model simulation affects rock strength anisotropy. Fig. 9 shows the modeled rock strengths of the posterior MAP solution (solid lines) derived from the entire dataset for the rocks: (4) Penrhyn slate (a), (5) slate (b) and (3) Moretown phyllite (c). The 95% prediction intervals due to the parameter and model simulation uncertainty are indicated with dark and light color regions, respectively (right plots). For clarity, the estimated 95% uncertainty ranges are displayed for only two confining stresses. Observation points at different confining stresses are represented with distinct colors and symbols. The U-shaped anisotropy curves demonstrate qualitatively how highly anisotropic these rocks are. The anisotropic HB model closely tracks the observed peak strengths at different orientation angles and levels of confining stresses for all rock materials. Our findings also reveal the potential existence of relatively large uncertainties in the peak strength for these highly anisotropic rocks. This outcome therefore highlights the relevance of recognizing the treatment of uncertainty of peak strengths in geotechnical analyzes. Similar findings have been reported by Gomes et al.[60] and Feng et al.[58] for uncertainty analysis in bedrock depth and *in situ* stresses, respectively.

Fig. 10 shows results of model simulations (left plots) and also illustrates how the marginal posterior probability density function of the parameters (Fig. 5) translates into 95% strength anisotropy predictive uncertainty (right plots) for the calibration datasets of the gneissic rocks: (2) gneiss (a) and (8) gneiss A (b). The results presented here are qualitatively very similar to those earlier outlined in Fig. 9 for the slates and phyllite. The proposed anisotropic model track the peak strength observations very well, although the stress ranges at different orientation angles are quite distinct for these rocks. Indeed, Fig. 10a indicates that different β-values hardly influence the observed peak strength, σ_1. The same is not true for gneiss A, which shows a much more anisotropic behavior. Similar to the phyllites by Ramamurthy et al.,[1] the anisotropy of gneiss A is reduced as a function of the confining stress. Note that parameter uncertainty appears to be a rather small contribution to total uncertainty. This trend is in agreement with the tight posterior parameter distributions of C_N and C_S in Fig. 5, especially for the (2) gneiss. Most part of the observations lies within the limits of the confidence intervals, supporting that the simulation uncertainty ranges should be statistically adequate.

The (1) Green river shale II has shown to be moderately anisotropic (Fig. 11a). The results show that the model predictions reproduce the observed σ_1-values quite well at different orientation angles and confining stresses. A relatively small under-prediction at $\beta = 30°$ is not represented in the model. As an example, notice that at $\sigma_c = 6.9$ and $\sigma_c = 68.9$ MPa, the 95% total prediction uncertainty bounds

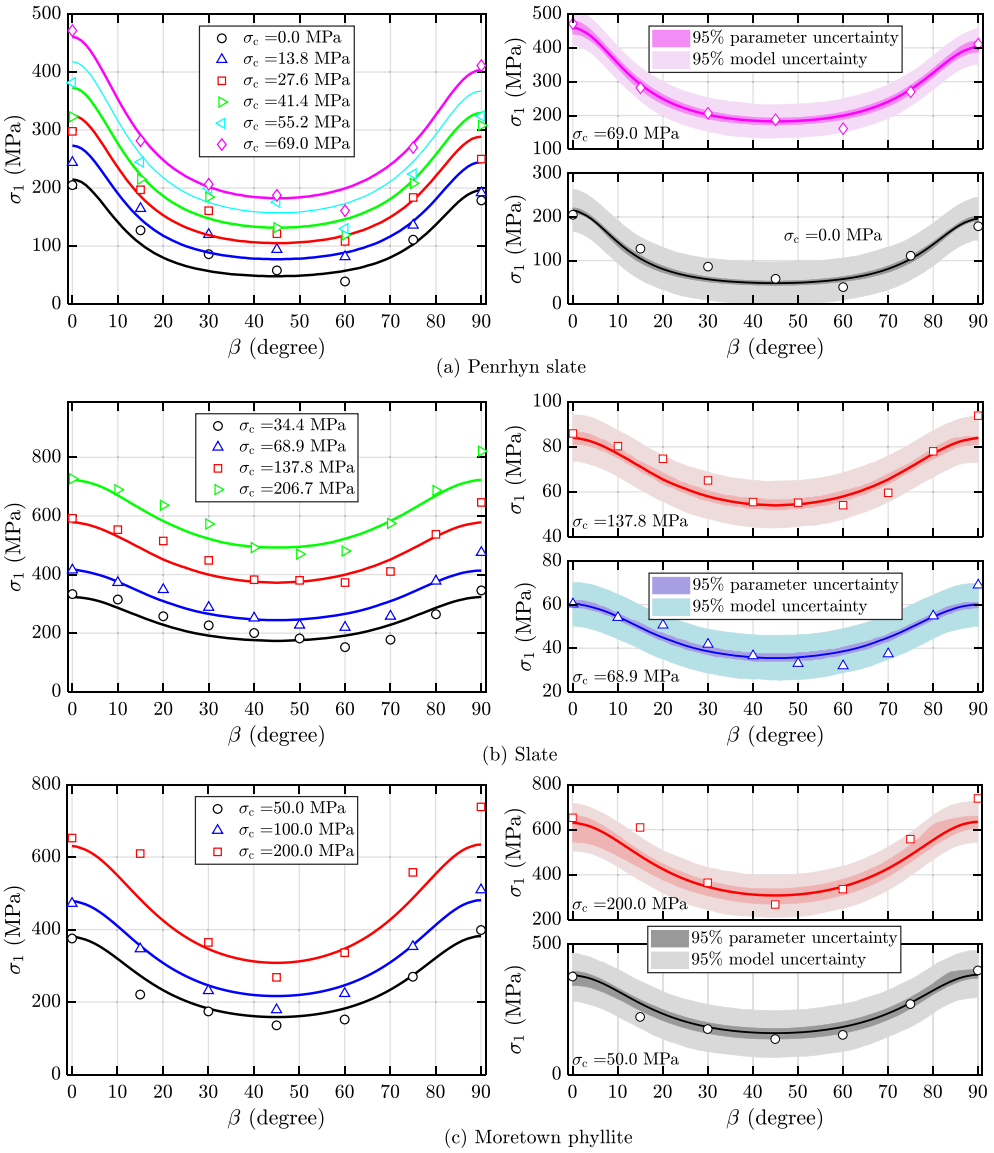

Fig. 9. Simulated rock strengths of the posterior MAP solution (solid lines) derived from the entire dataset for the (4) Penrhyn slate (a), (5) slate (b), and (3) Moretown phyllite (c). Examples of the 95% prediction intervals due to the parameter and model simulation uncertainty are indicated with dark and light color regions, respectively, in the right plots. Data points at different confining stresses are represented with distinct colors and symbols. (For interpretation of the references to color in this figure legend, the reader is referred to the web version of this article.)

bracket the peak strength data. As presented earlier, the total prediction uncertainty is quite large, indicating that the model and/or measurement uncertainty is remarkable. The 95% uncertainty region associated with parameter uncertainty is narrow and does not always bracket the strength data, suggesting that the model structure or the model input data might need additional improvement. Fig. 11b (left) shows comparisons between the deviatoric stresses σ_d of the triaxial test data performed on the (6) Tournemire shale rock and the predictions of the anisotropic HB model at different values of β (solid lines). Simulations include the confining stresses of σ_c = 20 MPa, σ_c = 40 MPa, and σ_c = 50 MPa. The results show that the model predictions are in good agreement with the observed σ_d-values, specially at β = 0° and when β has an intermediate angle. However, the anisotropic HB model underestimates σ_d at β = 90°. Additionally to our modeling outcomes, a visual comparison to the CALK model[70] shows that the posterior predictive simulations of σ_d are capable of capturing the measured strength data. As the CALK model is considerably more complex and uses three anisotropic parameters for inverse modeling, our results demonstrate that the proposed two-parameter model adequately represents the anisotropic behavior of the (6) Tournemire shale.

Finally, Fig. 11c compares the uniaxial compressive strength (UCS) model simulation results (solid black line) with the failure criterion of Fjær and Nes[14] (dashed red line) for the (7) Mancos shale. The error bars exhibit the uncertainty in the average UCS-value for each orientation angle, based on the estimated standard derivation of the collected data. The patchy weakness model of Fjær and Nes was specifically designed to assess heterogeneity on the anisotropic strength and visually shows a good match between model and observations. However, the HB anisotropic model does not fit the malicious small-scale variations of the rock strength induced by the measurement error and/or heterogeneity. Although these models differ fundamentally in their underlying philosophy, both methods receive similar performance in terms of rock strength predictions. In summary, results of both models indicate that the maximum strength of the (7) Mancos shale occurs when the major principal stress is either parallel or perpendicular to the anisotropy plane, while minimum strengths are found when the major principal stress direction and the anisotropy plane have an intermediate angle (between β = 30° and β = 50°). The model simulations also show that the 95% prediction uncertainty associated with only parameter

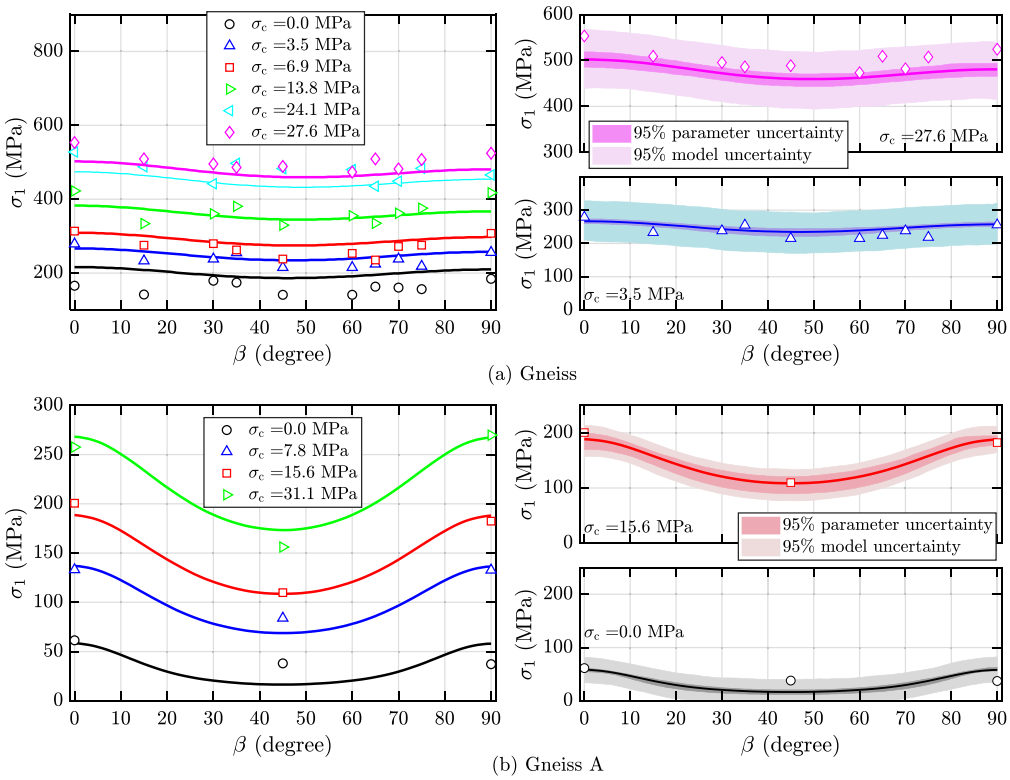

Fig. 10. Simulated rock strengths of the posterior MAP solution (solid lines) derived from the entire dataset for the gneissic rocks: (2) gneiss (a) and (8) gneiss A (b). Examples of the 95% prediction intervals due to the parameter and model simulation uncertainty are indicated with dark and light color regions, respectively, in the right plots. Data points at different confining stresses are represented with distinct colors and symbols. (For interpretation of the references to color in this figure legend, the reader is referred to the web version of this article.)

uncertainty (dark shaded area), and the 95% prediction uncertainty relative to the total error in terms of modeling residuals (light shaded area) are quite large, indicating that the model and/or measurement uncertainty is considerable.

The Bayesian framework used herein enables explicit treatment of uncertainty of the rock strength anisotropy. One of the major strengths of the proposed method is that, instead of merely assuming a known and deterministic rock strength, one can propagate its uncertainty to improve reliability in geotechnical analysis. Gomes et al.[61] have demonstrated that Bayesian analyzes coupled with MCMC simulations allows to determine more appropriate confidence limits for the factor of safety in slope stability analysis. We posit that probabilistic estimates of the rock strength anisotropy could improve model simulations in rock mechanics involving, for instance, circular tunnels,[81,82] and rock slope[83,84] and wellbore stability.[85] For instance, the anisotropic model proposed in this paper could be used as a strength criterion in geotechnical analysis. In this case, an ensemble of C_N and C_S would be propagated forward through existing numerical models. Since the uncertainty in the anisotropic parameters (Fig. 5) translates into uncertainty in rock strength (Figs. 9 to 11), this approach enables us to derive probabilistic estimates of safety factors, for example, thereby allowing proper recognition of the effect of strength anisotropy in stability assessments. Furthermore, the framework proposed here, while focused on homogeneous rock masses, could also support heterogeneity in anisotropy strength. In addition, our model formulation can be easily adapted to include the influence of the intermediate principal stress, σ_2. However, our findings suggest that the proposed anisotropic model can be applied to wide variety of rocks, with distinct degrees of anisotropy. The road to reliability in geotechnical analysis is a complex one. Without sound probabilistic techniques, that consider important sources of uncertainty on geotechnical analyzes, the chances of maintaining the deterministic *status quo* are high. This probabilistic analysis is beyond the scope of the current paper, but will be explored in future studies using the proposed model.

4. Conclusions

In this paper, we have introduced the different building blocks of an anisotropic Hoek–Brown model to predict the strength of anisotropic rocks. Our model builds on the isotropic Hoek–Brown failure criterion and calculates the strength anisotropy with a non-uniform scaling of the stress tensor. Two scaling factors (C_N and C_S) are used in our model to characterize adequately the effect of rock anisotropy. Bayesian inference was used to reconcile the predicted rock strength with experimental data. The following concluding remarks can be made:

- The anisotropic Hoek–Brown model simulations provide a good fit to the peak strength observations for both calibration and evaluation samples. The proposed model can reproduce the observed strength values quite well for rocks with different degrees of anisotropy (from low to high) at different orientation angles and confining stresses. Furthermore, our approach preserves the original Hoek–Brown strength criterion and definitions of the isotropic parameters.
- Bayesian analysis with the DREAM algorithm enables us to explore the posterior distribution of the anisotropic parameters, C_N and C_S, and their correlation. The general behavior of the posterior distributions of both parameters reveals that C_N and C_S are uncorrelated and that the marginal distributions are relatively tight and appear well resolved by the available rock strength data. Our approach highlighted parameter ranges for different anisotropic rocks, which could be used for constructing meaningful informative priors. Moreover, the parameter distributions derived will most likely characterize the different anisotropic rocks encountered in the real world.
- The conventional residual based likelihood function provides adequate statistical properties of the residuals. Analyzes of the

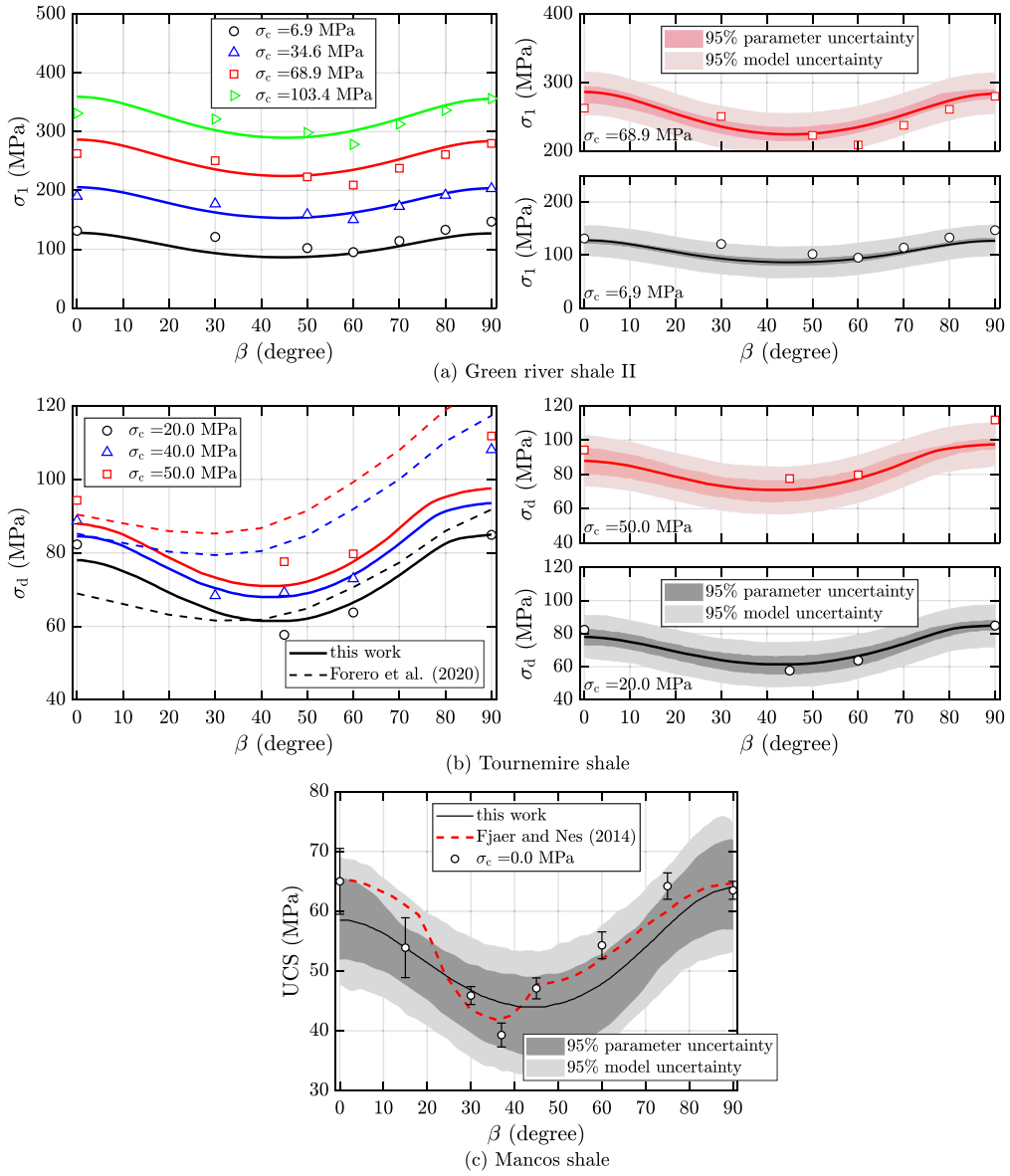

Fig. 11. Simulated rock strengths of the posterior MAP solution (solid lines) derived from the entire dataset for the (1) Green river shale II (a), (6) Tournemire shale (b) and (7) Mancos shale (b). Examples of the 95% prediction intervals due to the parameter and model simulation uncertainty are indicated with dark and light color regions, respectively, in the right plots. Data points are represented with distinct colors and symbols. (For interpretation of the references to color in this figure legend, the reader is referred to the web version of this article.)

autocorrelation functions, normality tests and plots of residuals as a function of the modeled peak stress sustained this conclusion.

- The split sampling approach indicates that the posterior estimates for the anisotropic parameters of the random samples match closely the MAP of the entire dataset of peak strength. Comparison of the values of R^2 and RMSE for the random samples and the full observations further supported the robustness of our methodology and inspires confidence in our findings.
- Our modeling results indicate that uncertainty in peak strength of anisotropic rocks can be quite large at different anisotropy plane orientations and confining stresses. This advocates the need for an explicit treatment of rock strength anisotropy uncertainty in rock mechanics studies.

CRediT authorship contribution statement

Guilherme J.C. Gomes: Methodology, Investigation, Visualization, Formal analysis, Software, Writing – original draft. **John H. Forero:** Methodology, Software, Database. **Eurípedes A. Vargas Jr.:** Conceptualization, Supervision. **Jasper A. Vrugt:** Validation, Formal analysis, Writing – review & editing.

Declaration of competing interest

The authors declare that they have no known competing financial interests or personal relationships that could have appeared to influence the work reported in this paper.

Acknowledgments

We wish to thank Miguel Mánica for help with the implementation of the proposed model. The authors greatly acknowledge financial support from the Brazilian National Council for Scientific and Technological Development, CNPq. The MATLAB code of the model presented herein is available upon request from the second author. This includes access to different datasets of this paper. We also want to thank helpful comments from two anonymous reviewers.

References

1. Ramamurthy T, Rao GV, Singh J. Engineering behaviour of phyllites. *Eng Geol*. 1993;33(3):209–225. http://dx.doi.org/10.1016/0013-7952(93)90059-L.
2. Amadei B. Importance of anisotropy when estimating and measuring in situ stresses in rock. *Int J Rock Mech Min Sci Geomech Abstr*. 1996;33(3):293–325. http://dx.doi.org/10.1016/0148-9062(95)00062-3.
3. Hoek E, Marinos P, Marinos V. Characterisation and engineering properties of tectonically undisturbed but lithologically varied sedimentary rock masses. *Int J Rock Mech Min Sci*. 2005;42(2):277–285. http://dx.doi.org/10.1016/j.ijrmms.2004.09.015.
4. Oda M, Nakayama H. Yield function for soil with anisotropic fabric. *J Eng Mech*. 1989;115(1):89–104. http://dx.doi.org/10.1061/(ASCE)0733-9399(1989)115:1(89).
5. Sayers CM. Stress-dependent seismic anisotropy of shales. *Geophysics*. 1999;64(1):93–98. http://dx.doi.org/10.1190/1.1444535.
6. Kuganenthira N, Zhao D, Anandarajah A. Measurement of fabric anisotropy in triaxial shearing. *Géotechnique*. 1996;46(4):657–670. http://dx.doi.org/10.1680/geot.1996.46.4.657.
7. Donath FA. Experimental study of shear failure in anisotropic rocks. *GSA Bull*. 1961;72(6):985–989. http://dx.doi.org/10.1130/0016-7606(1961)72[985:ESOSFI]2.0.CO;2.
8. McLamore R, Gray KE. The mechanical behavior of anisotropic sedimentary rocks. *J Eng Ind*. 1967;89(1):62–73. http://dx.doi.org/10.1115/1.3610013.
9. Horino F, Ellickson M. *A Method of Estimating the Strength of Rock Containing Planes of Weakness*. Report of Investigation 744; US Bureau of Mines; 1970.
10. Attewell PB, Sandford MR. Intrinsic shear strength of a brittle, anisotropic rock—I: Experimental and mechanical interpretation. *Int J Rock Mech Min Sci Geomech Abstr*. 1974;11(11):423–430. http://dx.doi.org/10.1016/0148-9062(74)90453-7.
11. Hoek E, Brown E. Empirical strength criterion for rock masses. *J Geotech Eng Div*. 1980a;106(GT9):1013–1035.
12. Niandou H, Shao JF, Henry JP, Fourmaintraux D. Laboratory investigation of the mechanical behaviour of Tournemire shale. *Int J Rock Mech Min Sci*. 1997;34(1):3–16. http://dx.doi.org/10.1016/S1365-1609(97)80029-9.
13. Saroglou H, Tsiambaos G. A modified hoek–brown failure criterion for anisotropic intact rock. *Int J Rock Mech Min Sci*. 2008;45(2):223–234. http://dx.doi.org/10.1016/j.ijrmms.2007.05.004.
14. Fjær E, Nes O. The impact of heterogeneity on the anisotropic strength of an outcrop shale. *Rock Mech Rock Eng*. 2014;47:1603–1611. http://dx.doi.org/10.1007/s00603-014-0598-5.
15. Ramamurthy T, Arora V. Strength predictions for jointed rocks in confined and unconfined states. *Int J Rock Mech Min Sci Geomech Abstr*. 1994;31(1):9–22. http://dx.doi.org/10.1016/0148-9062(94)92311-6.
16. Pietruszczak S, Lydzba D, Shao J. Modelling of inherent anisotropy in sedimentary rocks. *Int J Solids Struct*. 2002;39(3):637–648. http://dx.doi.org/10.1016/S0020-7683(01)00110-X.
17. Fjær E, Holt RM, Raaen AM, Risnes R, Horsrud P. *Petroleum Related Rock Mechanics, Vol. 53*. 2nd ed. London: Elsevier Science; 2008.
18. Meier T, Rybacki E, Backers T, Dresen G. Influence of bedding angle on borehole stability: A laboratory investigation of transverse isotropic oil shale. *Rock Mech Rock Eng*. 2015;48(4):1535–1546. http://dx.doi.org/10.1007/s00603-014-0654-1.
19. Yang D, Chanchole S, Valli P, Chen L. Study of the anisotropic properties of argillite under moisture and mechanical loads. *Rock Mech Rock Eng*. 2013;46(2):247–257. http://dx.doi.org/10.1007/s00603-012-0267-5.
20. Asadi M. Optimized mamdani fuzzy models for predicting the strength of intact rocks and anisotropic rock masses. *J Rock Mech Geotech Eng*. 2016;8(2):218–224. http://dx.doi.org/10.1016/j.jrmge.2015.11.005.
21. Dai Z, You T, Xu X, Zhu Q. Removal of singularities in Hoek–Brown criterion and its numerical implementation and applications. *Int J Geomech*. 2018;18(10):04018127. http://dx.doi.org/10.1061/(ASCE)GM.1943-5622.0001201.
22. Gao Z, Zhao J, Yao Y. A generalized anisotropic failure criterion for geomaterials. *Int J Solids Struct*. 2010;47:3166–3185. http://dx.doi.org/10.1016/j.ijsolstr.2010.07.016.
23. Gaede O, Karpfinger F, Jocker J, Prioul R. Comparison between analytical and 3D finite element solutions for borehole stresses in anisotropic elastic rock. *Int J Rock Mech Min Sci*. 2012;51:53–63. http://dx.doi.org/10.1016/j.ijrmms.2011.12.010.
24. Ghazvinian A, Vaneghi RG, Hadei M, Azinfar M. Shear behavior of inherently anisotropic rocks. *Int J Rock Mech Min Sci*. 2013;61:96–110. http://dx.doi.org/10.1016/j.ijrmms.2013.01.009.
25. Yilmaz I, Yucel Ö. Use of the core strangle test for determining strength anisotropy of rocks. *Int J Rock Mech Min Sci*. 2014;66:57–63. http://dx.doi.org/10.1016/j.ijrmms.2013.12.019.
26. Casagrande A, Carillo N. Shear failure of anisotropic materials. *J Boston Soc Civ Eng*. 1944;31:74–87.
27. Nova R. An extended cam clay model for soft anisotropic rocks. *Comput Geotech*. 1986;2(2):69–88. http://dx.doi.org/10.1016/0266-352X(86)90005-4.
28. Lee Y-K, Pietruszczak S, Choi B-H. Failure criteria for rocks based on smooth approximations to Mohr–Coulomb and Hoek–Brown failure functions. *Int J Rock Mech Min Sci*. 2012;56:146–160. http://dx.doi.org/10.1016/j.ijrmms.2012.07.032.
29. Jaeger JC. Shear failure of anistropic rocks. *Geol Mag*. 1960;97(1):65–72. http://dx.doi.org/10.1017/S0016756800061100.
30. Hoek E. Fracture of anisotropic rock. *J South Afr Inst Min Metall*. 1964;64(10):501–518.
31. Walsh JB, Brace WF. A fracture criterion for brittle anisotropic rock. *J Geophys Res (1896-1977)*. 1964;69(16):3449–3456. http://dx.doi.org/10.1029/JZ069i016p03449.
32. Amadei B. *Rock Anisotropy and the Theory of Stress Measurements, Vol. 2*. first ed. Springer-Verlag Berlin Heidelberg; 1983. http://dx.doi.org/10.1007/978-3-642-82040-3.
33. Duveau G, Shao J. A modified single plane of weakness theory for the failure of highly stratified rocks. *Int J Rock Mech Min Sci*. 1998;35(6):807–813. http://dx.doi.org/10.1016/S0148-9062(98)00013-8.
34. Tien YM, Kuo MC. A failure criterion for transversely isotropic rocks. *Int J Rock Mech Min Sci*. 2001;38(3):399–412. http://dx.doi.org/10.1016/S1365-1609(01)00007-7.
35. Sari M. An improved method of fitting experimental data to the Hoek–Brown failure criterion. *Eng Geol*. 2012;127:27–35. http://dx.doi.org/10.1016/j.enggeo.2011.12.011.
36. Sheorey P, Biswas A, Choubey V. An empirical failure criterion for rocks and jointed rock masses. *Eng Geol*. 1989;26(2):141–159. http://dx.doi.org/10.1016/0013-7952(89)90003-3.
37. Yoshida N, Morgenstern NR, Chan DH. A failure criterion for stiff soils and rocks exhibiting softening. *Can Geotech J*. 1990;27(2):195–202. http://dx.doi.org/10.1139/t90-023.
38. Ramamurthy T. Shear strength response of some geological materials in triaxial compression. *Int J Rock Mech Min Sci*. 2001;38(5):683–697. http://dx.doi.org/10.1016/S1365-1609(01)00035-1.
39. Saeidi O, Vaneghi RG, Rasouli V, Gholami R. A modified empirical criterion for strength of transversely anisotropic rocks with metamorphic origin. *Bull Eng Geol Environ*. 2013;72:257–269. http://dx.doi.org/10.1007/s10064-013-0472-9.
40. Hoek E, Brown E. Practical estimates of rock mass strength. *Int J Rock Mech Min Sci*. 1997;34(8):1165–1186. http://dx.doi.org/10.1016/S1365-1609(97)80069-X,
41. Martin CD, Kaiser PK, McCreath DR. Hoek-Brown parameters for predicting the depth of brittle failure around tunnels. *Can Geotech J*. 1999;36(1):136–151. http://dx.doi.org/10.1139/t98-072.
42. Li A, Lyamin A, Merifield R. Seismic rock slope stability charts based on limit analysis methods. *Comput Geotech*. 2009;36(1):135–148. http://dx.doi.org/10.1016/j.compgeo.2008.01.004.
43. Li A, Merifield R, Lyamin A. Effect of rock mass disturbance on the stability of rock slopes using the Hoek–Brown failure criterion. *Comput Geotech*. 2011;38(4):546–558. http://dx.doi.org/10.1016/j.compgeo.2011.03.003.
44. Hoek E, Carranza-Torres C, Corkum B. Hoek-Brown failure criterion—2002 edition. In: *NARMS-TAC Conf., Vol. 1*. North American Rock Mechanics; 2002:267–273.
45. Hoek E, Brown E. The Hoek–Brown failure criterion and GSI – 2018 edition. *J Rock Mech Geotech Eng*. 2019;11(3):445–463. http://dx.doi.org/10.1016/j.jrmge.2018.08.001.
46. Hoek E, Brown E. *Underground Excavations in Rock*. London: Institution of Mining and Metallurgys; 1980b.
47. Colak K, Unlu T. Effect of transverse anisotropy on the Hoek–Brown strength parameter "mi" for intact rocks. *Int J Rock Mech Min Sci*. 2004;41(6):1045–1052. http://dx.doi.org/10.1016/j.ijrmms.2004.04.004.
48. Shi X, Yang X, Meng Y, Li G. Modified Hoek–Brown failure criterion for anisotropic rocks. *Environ Earth Sci*. 2016;75(995):1–11. http://dx.doi.org/10.1007/s12665-016-5810-3.
49. Bagheripour MH, Rahgozar R, Pashnesaz H, Malekinejad M. A complement to Hoek–Brown failure criterion for strength prediction in anisotropic rock. *Geomech Eng*. 2011;3(1):61–81. http://dx.doi.org/10.12989/gae.2011.3.1.061.
50. Ismael MA, Imam HF, El-Shayeb Y. A simplified approach to directly consider intact rock anisotropy in Hoek–Brown failure criterion. *J Rock Mech Geotech Eng*. 2014;6(5):486–492. http://dx.doi.org/10.1016/j.jrmge.2014.06.003,
51. Contreras LF, Brown ET, Ruest M. BayesIan data analysis to quantify the uncertainty of intact rock strength. *J Rock Mech Geotech Eng*. 2018;10(1):11–31. http://dx.doi.org/10.1016/j.jrmge.2017.07.008.
52. Baecher GB, Christian JT. *Reliability and Statistics in Geotechnical Engineering*. England: John Wiley & Sons Ltd; 2003.
53. Bozorgzadeh N, Escobar MD, Harrison JP. Comprehensive statistical analysis of intact rock strength for reliability-based design. *Int J Rock Mech Min Sci*. 2018;106:374–387. http://dx.doi.org/10.1016/j.ijrmms.2018.03.005.
54. Board TR, National Academies of Sciences Engineering, and Medicine. In: Rix GJ, Wainaina N, Ebrahimi A, Bachus RC, Limas M, Sancio R, Fait B, Mayne PW, eds. *Manual on Subsurface Investigations*. Washington, DC: The National Academies Press; 2019. http://dx.doi.org/10.17226/25379.
55. Zhang L, Wu F, Zheng Y, Chen L, Zhang J, Li X. Probabilistic calibration of a coupled hydro-mechanical slope stability model with integration of multiple observations. *Georisk: Assess Manag Risk Eng Syst Geohazards*. 2018;12(3):169–182. http://dx.doi.org/10.1080/17499518.2018.1440317.
56. Contreras L-F, Brown ET. Slope reliability and back analysis of failure with geotechnical parameters estimated using Bayesian inference. *J Rock Mech Geotech Eng*. 2019;11(3):628–643. http://dx.doi.org/10.1016/j.jrmge.2018.11.008.

57. Yatheendradas S, Kirschbaum D, Nearing G, Vrugt JA, Baum RL, Wooten R, Lu N, Godt JW. BayesIan analysis of the impact of rainfall data product on simulated slope failure for north carolina locations. *Comput Geosci*. 2019;23:495–522. http://dx.doi.org/10.1007/s10596-018-9804-y.
58. Feng Y, Bozorgzadeh N, Harrison JP. BayesIan analysis for uncertainty quantification of in situ stress data. *Int J Rock Mech Min Sci*. 2020;134:104381. http://dx.doi.org/10.1016/j.ijrmms.2020.104381.
59. Zhu B, Hiraishi T, Pei H, Yang Q. Efficient reliability analysis of slopes integrating the random field method and a Gaussian process regression-based surrogate model. *Int J Numer Anal Methods Geomech*. 2020:1–24. http://dx.doi.org/10.1002/nag.3169.
60. Gomes GJC, Vrugt JA, Vargas Jr EA. Toward improved prediction of the bedrock depth underneath hillslopes: Bayesian inference of the bottom-up control hypothesis using high-resolution topographic data. *Water Resour Res*. 2016;52. http://dx.doi.org/10.1002/2015WR018147.
61. Gomes GJC, Vrugt JA, Vargas Jr EA, Camargo JT, Velloso RQ, van Genuchten MT. The role of uncertainty in bedrock depth and hydraulic properties on the stability of a variably-saturated slope. *Comput Geotech*. 2017;88:222–241. http://dx.doi.org/10.1016/j.compgeo.2017.03.016.
62. Feng Y, Harrison JP, Bozorgzadeh N. Uncertainty in in situ stress estimations: A statistical simulation to study the effect of numbers of stress measurements. *Rock Mech Rock Eng*. 2019;52:pages5071–5084. http://dx.doi.org/10.1007/s00603-019-01891-9.
63. Sari M, Karpuz C, Ayday C. Estimating rock mass properties using Monte Carlo simulation: Ankara andesites. *Comput Geosci*. 2010;36(7):959–969. http://dx.doi.org/10.1016/j.cageo.2010.02.001.
64. Fattahi H, Varmazyari Z, Babanouri N. Feasibility of Monte Carlo simulation for predicting deformation modulus of rock mass. *Tunn Undergr Space Technol*. 2019;89:151–156. http://dx.doi.org/10.1016/j.tust.2019.03.024.
65. Mazraehli M, Zare S. An application of uncertainty analysis to rock mass properties characterization at porphyry copper mines. *Bull Eng Geol Environ*. 2020;79:3721–3739. http://dx.doi.org/10.1007/s10064-020-01758-2.
66. Aladejare AE, Wang Y. Influence of rock property correlation on reliability analysis of rock slope stability: From property characterization to reliability analysis. *Geosci Front*. 2018;9(6):1639–1648. http://dx.doi.org/10.1016/j.gsf.2017.10.003.
67. Asem P, Gardoni P. BayesIan estimation of the normal and shear stiffness for rock sockets in weak sedimentary rocks. *Int J Rock Mech Min Sci*. 2019;124:104129. http://dx.doi.org/10.1016/j.ijrmms.2019.104129.
68. Bjureland W, Spross J, Johansson F, Anders Prästings A LS. Reliability aspects of rock tunnel design with the observational method. *Int J Rock Mech Min Sci*. 2017;98:102–110. http://dx.doi.org/10.1016/j.ijrmms.2017.07.004.
69. Ebrahimi MA, Ahmadi M, Ameri MJ. Application of unconditional simulation methods for quantifying the uncertainties in mud window design of gas reservoirs based on 3-dimensional mechanical earth modeling. *J Natl Gas Sci Eng*. 2020;76:103186. http://dx.doi.org/10.1016/j.jngse.2020.103186.
70. Forero JH, Gomes GJC, pedes A. Vargas Jr. E, ao FOLF, Velloso RQ. A cross-anisotropic elastoplastic model applied to sedimentary rocks. *Int J Rock Mech Min Sci*. 2020;132:104419. http://dx.doi.org/10.1016/j.ijrmms.2020.104419.
71. Mánica M, Gens A, Vaumat J, Ruiz DF. A cross-anisotropic formulation for elasto-plastic models. *Géotech Lett*. 2016;6(2):156–162. http://dx.doi.org/10.1680/jgele.15.00182.
72. Vrugt JA, ter Braak CJF, Clark MP, Hyman JM, Robinson BA. Treatment of input uncertainty in hydrologic modeling: Doing hydrology backward with Markov chain Monte Carlo simulation. *Water Resour Res*. 2008;44(12). http://dx.doi.org/10.1029/2007WR006720.
73. Vrugt JA, ter Braak CJF, Diks CGH, Robinson BA, Hyman JM, Higdon D. Accelerating Markov chain Monte Carlo simulation by differential evolution with self-adaptive randomized subspace sampling. *Int J Nonlinear Sci Numer Simul*. 2009;10(3):273–290. http://dx.doi.org/10.1002/esp.3423.
74. Vrugt JA. Markov chain Monte Carlo simulation using the DREAM software package: theory, concepts, and MATLAB implementation. *Environ Model Softw*. 2016;75:273–316. http://dx.doi.org/10.1016/j.envsoft.2015.08.013.
75. Jaeger J, Cook N, Zimmerman. R. *Fundamentals of Rock Mechanics*. 4th ed. Blackwell Publishing; 2007.
76. Donath F. Effects of cohesion and granularity on deformational behaviour of anisotropic rock. In: Doe B, Smith D, eds. *Studies in Mineralogy and Precambrian Geology*. Geological Society of America Memoir; 1972:95–128.
77. Rocscience. *RocLab User's Guide*. Toronto: Rocscience Inc; 2007 URL: www.rocscience.com Available free.
78. Fisher RA. Theory of statistical estimation. *Math Proc Camb Phil Soc*. 1925;22(5):700–725. http://dx.doi.org/10.1017/S0305004100009580.
79. Schoups G, Vrugt JA. A formal likelihood function for parameter and predictive inference of hydrologic models with correlated, heteroscedastic, and non-Gaussian errors. *Water Resour Res*. 2010;46(10). http://dx.doi.org/10.1029/2009WR008933.
80. Scharnagl B, Vrugt JA, Vereecken H, Herbst M. Inverse modelling of in situ soil water dynamics: investigating the effect of different prior distributions of the soil hydraulic parameters. *Hydrol Earth Syst Sci*. 2011;15(10):3043–3059. http://dx.doi.org/10.5194/hess-15-3043-2011.
81. Wang S, Sloan S, Tang C, Zhu W. Numerical simulation of the failure mechanism of circular tunnels in transversely isotropic rock masses. *Tunn Undergr Space Technol*. 2012;32:231–244. http://dx.doi.org/10.1016/j.tust.2012.07.003.
82. Wang T, Huang T. Anisotropic deformation of a circular tunnel excavated in a rock mass containing sets of ubiquitous joints: Theory analysis and numerical modeling. *Rock Mech Rock Eng*. 2014;47:643–657. http://dx.doi.org/10.1007/s00603-013-0405-8.
83. Yang T, Shi W, Wang P, Liu H, Yu Q, Li Y. Numerical simulation on slope stability analysis considering anisotropic properties of layered fractured rocks: a case study. *Arabian Journal of Geosciences*. 2015;5:5413–5421. http://dx.doi.org/10.1007/s12517-014-1609-2.
84. Yeh P, Lee KZ-Z, Chang K. 3D effects of permeability and strength anisotropy on the stability of weakly cemented rock slopes subjected to rainfall infiltration. *Eng Geol*. 2020;266:105459. http://dx.doi.org/10.1016/j.enggeo.2019.105459.
85. Bautmans P, Fjær E, Horsrud P. The effect of weakness patches on wellbore stability in anisotropic media. *Int J Rock Mech Min Sci*. 2018;104:165–173. http://dx.doi.org/10.1016/j.ijrmms.2018.01.016.